

Contents lists available at ScienceDirect

Journal of the Mechanics and Physics of Solids

journal homepage: www.elsevier.com/locate/jmps





The Green's function based thermoelastic analysis of spherical geothermal tanks in a semi-infinite domain

Chunlin Wu a,b, Tengxiang Wang b, Huiming Yin b,*

- ^a Shanghai Institute of Applied Mathematics and Mechanics, Shanghai Key Laboratory of Mechanics in Energy Engineering, Shanghai Frontier Science Center of Mechanoinformatics, School of Mechanics and Engineering Science, Shanghai University, Shanghai, 20072, People's Republic of China
- ^b Department of Civil Engineering and Engineering Mechanics, Columbia University, 610 Seeley W. Mudd 500 West 120th Street, New York, 10027, United States of America

ARTICLE INFO

Keywords: Bi-material Green's functions Eshelby's equivalent inclusion method Eigenstrain Geothermal system Thermoelastic analysis

ABSTRACT

When an underground heat exchanger is subjected to a surface load on the ground and temperature change inside, the stress transfer between the thermal tank and the earth may cause the deformation and destruction of the tank. The bi-material thermoelastic fundamental solution of two-jointed dissimilar half-spaces is applied to elastic and thermal analysis of spherical heat storage tanks, where the continuity equations at the bi-material interface are satisfied. Using Hadamard's regularization in the x_3 direction, the two-dimensional bi-material thermoelastic fundamental solution can be obtained. By changing the material constants, the fundamental solution for a semi-infinite domain or an infinite domain with a single material can be recovered. In general, the storage tanks and soil exhibits different thermal and mechanical properties. A dual equivalent inclusion method (DEIM) is proposed to simulate the material mismatch of thermal conductivity and elasticity with continuously distributed eigen-temperature-gradients and inelastic eigenstrains on the tanks, respectively. Using the analytical domain integrals, no mesh is required for inhomogeneities. Due to the boundary effects and inhomogeneity interactions, the eigen-fields are expanded at the center of each inhomogeneity using the Taylor series with tailorable accuracy. The DEIM is verified by the finite element method and demonstrated by the geothermal applications using uniform, linear, or quadratic orders of eigenfields. For a spherical heat exchanger in an infinite homogeneous domain, DEIM provides the exact solutions of the thermoelastic fields for a uniform heat source and a uniform far-field heat

1. Introduction

Spherical underground heat exchangers have been employed to store heat energy and also, interact with surrounding soil via heat exchange (Wang et al., 2022) as the ground temperature profile is relatively stable under a certain depth, which exhibits great potential for the thermal management of buildings with improved energy efficiency among other environmental benefits. Geothermal systems have drawn significant attention both in research and industry field (Yin et al., 2013, 2021). The thermal analysis regarding geothermal tank systems has been rigorously investigated through experimental, analytical and numerical analysis (Kuang et al., 2003; Qu et al., 2010; Benzaama et al., 2018; Li et al., 2015; Wang et al., 2022). The stress transfer for underground structures,

E-mail addresses: cw3056@columbia.edu (C. Wu), tw2520@columbia.edu (T. Wang), yin@civil.columbia.edu (H. Yin).

^{*} Corresponding author.

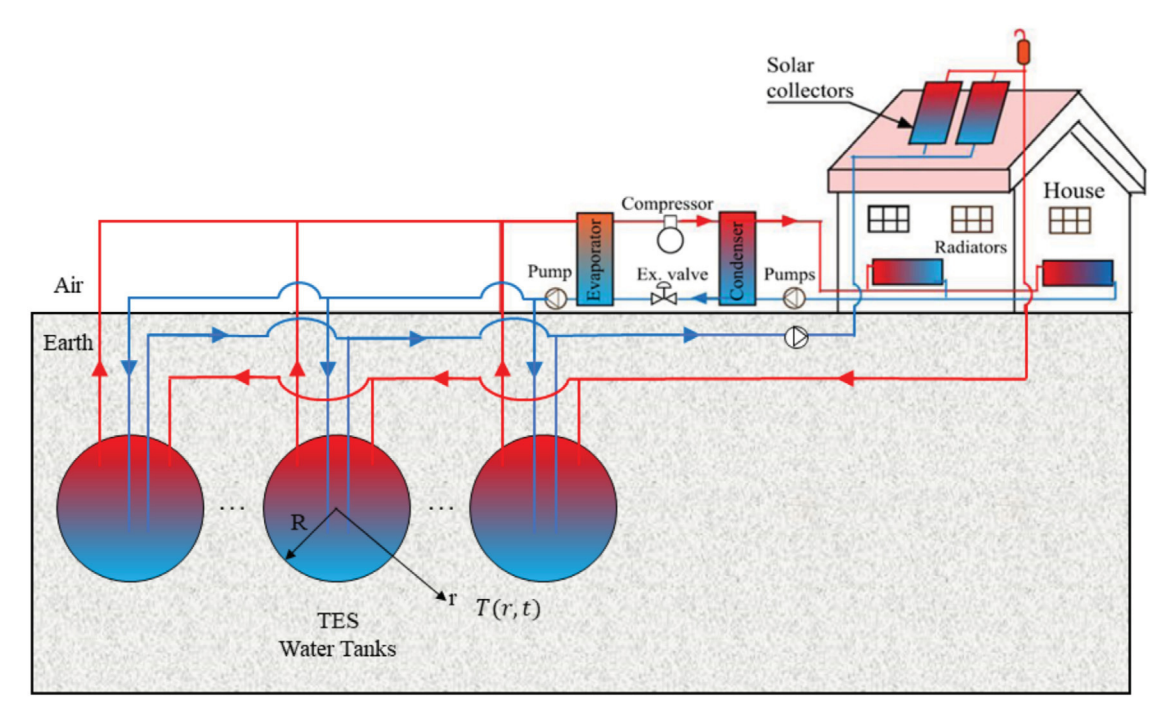


Fig. 1. Schematic illustration of a bi-directional geothermal system using multiple spherical thermal energy storage tanks.

particularly for piping systems (Kramer and Basu, 2014; Hwang et al., 2020), has also received significant attention for damage by thermal stress induced by temperature change.

Fig. 1 shows a bi-directional geothermal system working for both a thermal energy storage and a heat sink, which is designed to manage indoor temperature and reduce related energy consumption (Wang et al., 2022). Multiple tanks can be used for improved performance and capacity. They can store heat in the surrounding ground in summer and use it in winter for seasonal thermal management. The performance of such a system depends on the heat transfer process. In our recent work (Wang et al., 2022), we have investigated the effects of thermal conductivity, and depth of a single spherical geothermal tank considering temperature gradients and prescribed heat source by heat pumps. In addition to thermal analysis of heat flows, it is essential to investigate the thermoelastic effects introduced by temperature changes, as such effects may cause potential damage to neighboring structures and bring about safety issues. Particularly, the understanding of thermoelastic effects can help engineers to optimize designs and improve the overall performance of the bi-directional geothermal system.

As the thermal response of a geothermal system is critical to the energy performance; the stress transfer analysis of the geothermal system addresses its safety and design specification as underground thermal tanks are sometimes under static and dynamic surface loading like vehicle parking and moving, respectively. The fundamental solution of a semi-infinite space with a concentrated point force can be firstly found in Boussinesq's solution (Boussinesq, 1885), where a point force is applied perpendicular to and on the plane surface of an isotropic half-space. Subsequently, for a two-jointed half-spaces, Head (1953) and others (Michell, 1899; Love, 2013) utilized harmonic potentials to derive the elastic solution with different interface conditions, i.e stress transmission and completely weld. Mindlin (1936) relaxed the condition of Boussinesq's problem and proposed the fundamental solution, namely the Mindlin's solution, to an arbitrarily concentrated point force inside the half-space with a traction-free boundary condition. Later, a concise form of the Mindlin's solution was derived from Galerkin's stress vector (Mindlin and Cheng, 1950a) and Rongved (1955a) achieved the solution of the same problem as Mindlin's but with a fixed boundary condition, which existed in fluid mechanics as well (Lorentz, 1907). Rongved (1955b) further generalized the case to a concentrated force interior to one of the two-jointed dissimilar semi-infinite solids. For hydrostatic inclusions, Mindlin and Cheng (1950b) and Sen (1951) considered the thermal-elastic stresses.

In the literature, pioneers (Yu et al., 1992; Yu and Sanday, 1991; Singh et al., 1999; Tinti and Armigliato, 1998) have extended the previous semi-infinite solution for bi-materials. Walpole (1996) and Huang and Wang (1991) generalized (Collins, 1960) and derived the explicit fundamental solution for bi-materials with two interface conditions by method of images. By adjusting the material properties of two materials, the bi-material fundamental solution can be reduced to half-space solutions such as the celebrated Lorentz's and Mindlin's problem. In addition, the bi-material fundamental solution to Stoke's flow (Huang and Wang, 1991) was derived with in-compressible Poisson's ratio. Other contributions on bi-material elasticity can be found in Liu et al. (2011) and Wu et al. (2022).

As for the research on isotropic thermoelastic problems, Biot (1956) acquired the solution composed of four potential functions through the extension of the Papkovitch–Neuber solution. Subsequently, Verruijt (1969) proved the completeness of Biot's general

solution. For transversely isotropic materials, the authors (Podil'chuk and Sokolovskii, 1994) proposed the solution with four potential functions, where the last one is governed by the non-homogeneous differential equation. Nowacki (1986) obtained the full-space fundamental solution of a concentrated point heat source, and Barber (1992) summarized the derivation for both two-and three-dimensional problems.

Regarding application of bi-materials, Yu et al. (1992) extended (Yu and Sanday, 1991) and followed Goodier's method of integration (Goodier, 1937) to derive bi-material Green's function with prescribed temperature change and the authors investigated thermal stresses caused by a spherical inclusion. Sharma (1958) provided the integral-form solution to a transversely isotropic semi-infinite domain. Hou et al. (2008a,b) followed Chen et al. (2004) and achieved solutions of full space and bi-materials. Hou's group (Hou et al., 2013b,a) pointed the inconvenience to apply previous fundamental solutions (Haojiang et al., 2000) to certain boundary value problems (BVPs) because they are generally combined with both harmonic and non-harmonic potential functions. Therefore, they proposed a solution composed of three harmonic potential functions (Hou et al., 2013b,a), which can be used to deal with the BVPs.

Thanks to Eshelby's celebrated work (Eshelby, 1957, 1959) of the equivalent inclusion method (EIM), the original inclusion/inhomogeneity problem can be completely and mathematically transformed as a process to solve the continuously distributed eigenstrain field. Such treatment avoids trivial procedures to handle interfacial continuity equations as displacements and tractions, which saves efforts in both computations as well as preprocess of mesh. As Yu et al. (1992) concluded that when the inclusion is close to a free-surface (bi-material interface in the case study), both the thermal and elastic fields can be greatly disturbed due to the boundary effects, where the image terms become dominant. As for inhomogeneity problems, Mura (1987) mentioned the inaccuracy to use merely constant eigenstrain under inhomogeneity interactions and the authors suggested using a higher-order polynomials, i.e. the Taylor series expansion at the center of inhomogeneities. Following Mura's work, Liu et al. (2015) indicated intensive boundary effects when the ratio of distance and radius of spherical particles becomes small; Wu et al. (2023) observed that the intensive boundary effects cause angle shift of maximum stress concentration. Dong et al. (2020) investigated plane strain elastic responses of the thin film-substrate system with rough surfaces under contact loading, where the authors combined EIM and conjugate gradient method (CGM) to handle layered volume and surface pressure, respectively. Zhou et al. (2011a) studied the effect of hard coatings over a substrate with cuboid inhomogeneities. And the coating layers are discretized into the grid elements with constant eigenstrain to deal with the material mismatch of the substrate. Subsequently, Zhou's group extends to arbitrarily shaped inhomogeneities (Zhou et al., 2011b). Following Zhou's works, Wei et al. (2016) proposed a fatigue model to understand crack propagation considering cyclic load and initial misfit strain. Other works related to Eshelby's EIM on a semi-infinite domain can refer to the review paper (Zhou et al., 2013).

This paper investigates the thermoelastic behavior of thermal tanks in the ground, which are considered inhomogeneities exhibiting different thermoelastic properties, specifically (i) thermal conductivity; (ii) thermal expansion coefficients and (iii) stiffness, from the surrounding earth. Hence, the original equivalent inclusion method is further extended to couple both thermal and elastic fields, namely the dual EIM (DEIM). In Eshelby's EIM (Eshelby, 1957; Mura, 1987), the thermal strain is typically considered as an eigenstrain. However, a heat source causes temperature variation over the whole domain, which is corresponding to eigenstrain in the whole domain, so it is not effective in separately addressing the thermal strain. In DEIM, polynomial eigen-temperature gradients (ETG) and eigenstrains are introduced to simulate the material mismatch at tailorable accuracy by using uniform, linear and quadratic forms of ETG and eigenstrains on the particle domain only. The complete bi-material thermoelastic fundamental solution for a point heat source in the Cartesian coordinate, which is expressed in terms of potential functions, is used to calculate the thermal stress, and the dual equivalent inclusion conditions on thermal conduction and stress equilibrium are set up on the inhomogeneity to solve for the eigen-fields and then thermoelastic fields.

In the following, Section 2 presents the problem statement for the boundary value problems with fully bonded interfaces. Section 3 rederives the bi-material thermoelastic fundamental solution in the tensor form (Hou et al., 2013b), which is convenient and straightforward for domain integrals and programming. Subsequently, the DEIM is presented with eigen-temperature-gradients and eigenstrain. Although the case studies focus on a semi-infinite domain, in Section 5, the scheme is verified and demonstrated with the finite element method (FEM) with two-jointed dissimilar half-spaces. Through adjusting the material coefficients, the bi-material interface conditions can reduce to the same as Mindlin's and Rongved's problems. In Section 5, the effects of stiffness, relative position, and dimension of spherical tanks are investigated with and without thermal fields. Section 6 presents thermoelastic solutions for a single spherical heat exchanger in an infinite solid subjected to a uniform heat source or heat flux, respectively. Finally, some conclusive remarks are provided in Section 7.

2. Problem statement

Consider a two-jointed full space $\mathcal D$ containing multiple subdomains Ω^I , and in general, the two phases (the upper $\mathcal D^+$ and the lower $\mathcal D^-$) exhibit different mechanical properties. Regarding the thermoelastic problem, let $\mathcal C$, $\mathcal A$ and $\mathcal K$ denote the isotropic stiffness tensor, thermal modulus, and thermal conductivity, respectively. Here the thermal modulus $\mathcal A=(3\lambda+2\mu)\alpha$, where λ,μ,α are the two Lame constants and thermal expansion ratio, respectively. Shown in Fig. 2, the superscripts ', ", and I denote properties of the upper, lower half-space and the Ith inhomogeneity, respectively. Without the loss of any generality, the bi-material interface is selected as x_1-x_2 plane when $x_3\equiv 0$. The continuity assumptions are made on (i) the bi-material interface and (ii) interfaces between subdomains Ω^I and matrix $\mathcal D$ for both stress transfer and heat conduction as Eq. (1),

$$u_{i}(\mathbf{x}^{+}) = u_{i}(\mathbf{x}^{-}), \quad \sigma_{ij}(\mathbf{x}^{+})n_{j}(\mathbf{x}^{+}) = \sigma_{ij}(\mathbf{x}^{-})n_{j}(\mathbf{x}^{-})$$

$$T(\mathbf{x}^{+}) = T(\mathbf{x}^{-}), \quad q_{i}(\mathbf{x}^{+}) = q_{i}(\mathbf{x}^{-})$$
(1)

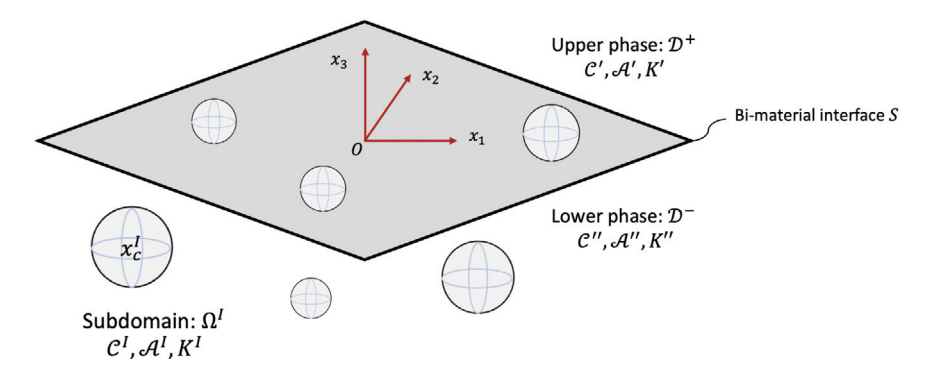


Fig. 2. Schematic illustration of the boundary value problem for a two-jointed half-spaces containing inhomogeneities.

where the superscripts "+" and "-" represent the inward and outward surface of the interfaces between subdomain and matrix and bi-material interface, respectively; \mathbf{n} denotes the unit surface normal vector and, specifically, $\mathbf{n} = (0,0,\pm 1)$ at bi-material interface S. Combining Navier's governing equation, a boundary value problem can be formulated and solved through the domain discretization method (on subdomain surface or subdomain volume). As introduced in the last section, Eshelby transformed the conventional BVPs to the determination of eigen-fields analytically, which elegantly avoided the discretization procedures in numerical methods. By virtue of Eshelby's method, this paper utilizes the thermal, elastic, and thermoelastic Green's functions for an infinite bi-material domain to handle the thermoelastic inhomogeneity problem by determining the thermal (ETG) and elastic (eigenstrain) eigen-fields and then derive the thermal stress caused by underground heat exchange.

The Green's functions define the temperature or displacement response of any field point x caused by a point source at x'. Given a point heat source $\delta(x')$ as a Dirac Delta function, the temperature and displacement variations can be written as,

$$T(\mathbf{x}) = G(\mathbf{x}, \mathbf{x}')\delta(\mathbf{x}'); \quad u_i(\mathbf{x}) = G_i(\mathbf{x}, \mathbf{x}')\delta(\mathbf{x}')$$
(2)

where the thermal Green's function G is a scalar function; while the thermoelastic Green's function G_i is a vector function.

Given a point force source $f_i(\mathbf{x}') = n_i \delta(\mathbf{x}')$ as a unit concentrated force in the direction \mathbf{n} , the displacement variation can be written as,

$$u_i(\mathbf{x}) = G_{ii}(\mathbf{x}, \mathbf{x}') f_i(\mathbf{x}') \tag{3}$$

where the elastic Green's function G_{ij} is a second-rank tensor function. Although the same symbol is used for all three Green's functions, they are differentiated by the rank of 0, 1, and 2 for thermal, thermoelastic, and elastic Green's functions, respectively. For a bi-material domain, the Green's functions shall be defined in accordance with the material domains of the source and field points, which will be demonstrated in the next section. Some specific Green's functions are also provided in Appendix B.

3. Formulation

3.1. Elastic and thermal fundamental solutions for two-jointed dissimilar half-spaces

Following the assumption in Section 2, when one concentrated force is applied at the arbitrary interior point of the upper phase \mathcal{D}^+ , Walpole (1996) derived the solution based on nuclei of strain, while Huang and Wang (1991) obtained it through the extension of the Papkovitch–Neuber solution. However, both of them applied the method of image, whose basis is the superposition of two fields, also known as double force (Yu et al., 1992). Therefore, the fundamental solution contains the Kelvin's solution and the image parts. Wu et al. (2022) completed all cases of the solution when the source $x_3' < 0$ by virtue of mathematical equivalence and the solution is listed as Eq. (4),

$$4\pi\mu^{w}G_{ij}^{y}(\mathbf{x},\mathbf{x}') = \begin{cases} (\delta_{ij}\phi - \frac{\psi_{,ij}}{4(1-v^{w})}) + A^{y}\overline{\phi}\delta_{ij} + \chi B^{y}(\delta_{i3}\delta_{jk} - \delta_{ik}\delta_{j3})\overline{\alpha}_{,k}^{y} \\ - C^{y}x_{3} \left[Q_{J}\overline{\psi}_{,ij3} + 4(1-v^{w})\delta_{j3}\overline{\phi}_{,i} + 2(1-2v^{w})\delta_{i3}Q_{J}\overline{\phi}_{,j} - Q_{J}x_{3}\overline{\phi}_{,ij}\right] & x_{3}'x_{3} \ge 0 \\ - D^{y}Q_{I}Q_{J}\overline{\psi}_{,ji} - (G^{y} + B^{y})Q_{J}\overline{\beta}_{,ij}^{y} \\ (\delta_{ij}\phi - \frac{\psi_{,ij}}{4(1-v^{w})}) + A^{y}\phi\delta_{ij} + \chi B^{y}(\delta_{i3}\delta_{jk} - \delta_{ik}\delta_{j3})\alpha_{,k}^{y} \\ - D^{y}\psi_{,ij} - \chi x_{3}F^{y}\alpha_{,ij}^{y} - (G^{y} + B^{y})Q_{I}\beta_{,ji}^{y} \end{cases} \qquad x_{3}'x_{3} < 0 \end{cases}$$

where the superscripts w, y and χ change according to the position of the source point that: (i) when $x_3' \ge 0$, w = ', y = u and $\chi = 1$ and (ii) when $x_3' < 0$, w = '', y = l and $\chi = -1$; $\psi = |\mathbf{x} - \mathbf{x}'|$ is Galerkin's distance vector and $\phi = \frac{1}{w}$; the $\overline{(.)}$ stands for the image terms,

i.e. $\overline{\psi} = |\mathbf{x} - \overline{\mathbf{x}}'|$, where $\overline{x}_i' = Q_I x_i'$ and Q = (1, 1, -1) handles a negative partial derivative with respect to the third direction. Note that Mura's index notation is used for $Q_I x_i'$ that the term with an uppercase index is a coefficient for the term with the lower case index and does not trigger the summation as the repeated lower case indices (Mura, 1987). When $x_3' \ge 0$, the material coefficients $A^u - G^u$ of D^+ are provided as Eq. (5),

$$A^{u} = \frac{\mu' - \mu''}{\mu' + \mu''}, \quad B^{u} = \frac{2\mu'(1 - 2\nu')(\mu' - \mu'')}{(\mu' + \mu'')(\mu' + \mu''(3 - 4\nu'))}$$

$$C^{u} = \frac{\mu' - \mu''}{2(1 - \nu')(\mu' + (3 - 4\nu')\mu'')}, \quad D^{u} = \frac{3 - 4\nu'}{2}C$$

$$F^{u} = \frac{2\mu'(\mu'(1 - 2\nu'') - \mu''(1 - 2\nu'))}{(\mu' + \mu''(3 - 4\nu'))(\mu'' + \mu'(3 - 4\nu''))}$$

$$G^{u} = \frac{\mu'(\mu''(1 - 2\nu'')(3 - 4\nu') - \mu'(1 - 2\nu')(3 - 4\nu''))}{(\mu' + \mu''(3 - 4\nu'))(\mu'' + \mu'(3 - 4\nu''))}$$
(5)

In the same fashion, the material coefficients A^l-G^l can be acquired by switching the sequence of material properties. For example, $B^l=\frac{2\mu''(1-2\nu'')(\mu''-\mu')}{(\mu''+\mu'')(\mu'''+\mu''(3-4\nu''))}$, which is based on the mathematical equivalency. Other components in addition to ψ and ϕ are provided as Eq. (6),

$$\alpha^{u} = \ln[x'_{3} - x_{3} + \psi], \quad \overline{\alpha}^{u} = \ln[x'_{3} + x_{3} + \overline{\psi}]
\beta^{u} = (x'_{3} - x_{3})\alpha^{u} - \psi, \quad \overline{\beta}^{u} = (x'_{3} + x_{3})\overline{\alpha}^{u} - \overline{\psi}
\alpha^{l} = \ln[-x'_{3} + x_{3} + \psi], \quad \overline{\alpha}^{l} = \ln[-x'_{3} - x_{3} + \overline{\psi}]
\beta^{l} = (-x'_{3} + x_{3})\alpha^{l} - \psi, \quad \overline{\beta}^{l} = (-x'_{3} - x_{3})\overline{\alpha}^{l} - \overline{\psi}$$
(6)

where Eq. (6) contains 4 branches of potential functions of α and β , which are partial integration of harmonic potential ϕ with respect to direction z at the first and second orders, respectively (Yin et al., 2022). In the literature, they have been named the Boussinesq's displacement potentials or ϕ_{-1} and ϕ_{-2} (Barber, 1992). The differences among the 4 branches are integral limits and image terms, i.e $\overline{\alpha}^u = \int_{\infty}^{x_3} \overline{\phi}(x_1, x_2, t) \, dt$ and $\alpha^u = \int_{x_3}^{-\infty} \phi(x_1, x_2, t) \, dt$.

When the two phases exhibit the same properties, all material coefficients of A^u - G^u in Eq. (5) become zero, and the fundamental solution reduces to Kelvin's solution. For applications to a semi-infinite domain with a free or fixed surface, one can assign $C' \equiv 0$ or ∞ , respectively; hence, Mindlin's and Lorentz's problems are particular cases of the bi-material fundamental solution (Yin et al., 2022). Similarly, the thermal Green's function has been given in our recent work (Wang et al., 2022) as Eq. (4). By adjusting the material constants, one can obtain the Green's function for semi-infinite domains, and an infinite homogeneous domain as well, which are summarized in Appendix B.

3.2. Thermoelastic fundamental solution for two-jointed dissimilar half-spaces

Hou et al. (2013b) have derived the thermoelastic general solution in the cylindrical coordinate by using the axisymmetry of a single heat source, in which three harmonic potentials are expressed in combinations of α and β in Eq. (6). However, it is not convenient to use it for the case with many dispersed sources in the loss of the overall axisymmetry. This subsection will derive the bi-material thermoelastic fundamental solution in the Cartesian coordinate based on 3 harmonic potentials V_i (i = 1, 2, 3) as well (Hou et al., 2013b). Without the loss of any generality, in the derivation process, the source point $x_3' \ge 0$ is assumed and the other cases can be acquired similarly by switching the material parameters. Using the same notation (Hou et al., 2013b), the displacements are expressed as below,

$$2\mu u_1 = \mathcal{U}_{1,1} + x_3 \mathcal{U}_{2,1}, \qquad 2\mu u_2 = \mathcal{U}_{1,2} + x_3 \mathcal{U}_{2,2}$$

$$2\mu u_3 = \mathcal{U}_{1,3} - (3 - 4\nu)\mathcal{U}_2 + x_3 \mathcal{U}_{2,3} + 4(1 - \nu)\mathcal{U}_3$$
(7)

where $\Gamma = \frac{4(1-\nu)\mu}{(1-2\nu)\mathcal{A}}$ is one coefficient associated with the thermal modulus and Poisson's ratio; the potential functions \mathcal{U}_i (i=1,2,3) are provided as below,

(a) When $x_3'x_3 \ge 0$, the source and field points are in the same material phase,

$$\mathcal{U}_1 = \overline{A}_{11}\overline{\beta}^u + \overline{A}_{12}\overline{\alpha}^u + A_{11}\beta^{u'} + A_{12}\alpha^{u'}, \qquad \mathcal{U}_2 = \overline{A}_{21}\overline{\alpha}^u + A_{21}\alpha^{u'} + \overline{A}_{22}\overline{\phi}, \quad \mathcal{U}_3 = A_3\alpha^{u'} + \overline{A}_3\overline{\alpha}^u$$
 (8)

(b) when $x_3'x_3 < 0$, the source and field points are in the different material phases,

$$\mathcal{U}_1 = A'_{11}\beta^{u'} + A'_{12}\alpha^{u'}, \quad \mathcal{U}_2 = A'_{21}\alpha^{u'} + A'_{22}\phi, \quad \mathcal{U}_3 = A'_3\alpha^{u'}$$
(9)

where $\overline{\alpha}^u$ and $\overline{\beta}^u$ are potential functions given in Eq. (6); $\alpha^{u'}$ and $\beta^{u'}$ are created to handle continuity conditions when the source and field points are at the same height $x_3 = x_3'$, which contains the sign function $S(x) = \begin{cases} 1 & x > 0 \\ -1 & x < 0 \end{cases}$,

$$\beta^{u'} = S(x_3 - x_3') \ln[\psi + S(x_3 - x_3')] - \psi, \quad \alpha^{u'} = S(x_3 - x_3') \ln[\psi + S(x_3 - x_3')]$$
(10)

and the continuity equations at $x_3 = x_3'$ are the continuity of all components of displacement and traction. The derivation process has been presented in Hou et al. (2013b), therefore, the result is directly applied and the details are not repeated below. From the potential function \mathcal{U}_3 , one can also obtain the temperature as,

$$\theta = \frac{\Gamma}{2\mu} \mathcal{V}_{3,3} \tag{11}$$

To determine the coefficients in the potential functions, three equations can be obtained with the continuity conditions at $x_3 = x_4'$,

$$\begin{cases} A_{12} + A_{21}x_3' = 0 & \text{continuity of } u_1 \text{ and } u_2 \\ A_{11} - (3 - 4v)A_{21} + 4(1 - v)A_3 = 0 & \text{continuity of } u_3 \\ A_{11} - (1 - 2v)A_{21} + 2(1 - v)A_3 = 0 & \text{continuity of } \gamma_{31} \text{ and } \gamma_{32} \end{cases}$$

$$(12)$$

where one can obtain the relationship of A_{11} , A_{12} , A_{21} with A_3 as,

$$A_{11} = -A_3, \quad A_{12} = -A_3 x_3', \quad A_{21} = A_3$$
 (13)

where A_3 is the coefficient yet to be determined based on the thermal continuity equations. On the other hand, the temperature field can be independently determined from the thermal analysis, and the stress field can be derived by temperature change. Therefore, the coefficients A_3 , $\overline{A_3}$ and A_3' can be obtained through the thermal Green's function as,

$$A_{3} = \frac{1}{8\pi K'} \frac{(1 - 2v')A'}{1 - v'}, \quad \overline{A}_{3} = \frac{1}{8\pi K'} \frac{(1 - 2v')A'}{1 - v'} \frac{K' - K''}{K' + K''}, \quad A'_{3} = \frac{1}{4\pi (K' + K'')} \frac{(1 - 2v'')A''}{1 - v''}$$

$$(14)$$

Replacing the components in continuity equation Eq. (1) with displacements as Eqs. (7)–(9), eight subsequent equations can be obtained, where the derivation details are elaborated in Appendix A,

$$\begin{cases} A_{11} + \overline{A}_{11} &= \frac{\mu'}{\mu''} A'_{11} & \text{continuity of } u_1 \text{ and } u_2 \\ A_{12} - \overline{A}_{12} &= \frac{\mu'}{\mu''} A'_{12} & \text{continuity of } u_1 \text{ and } u_2 \\ (A_{11} - \overline{A}_{11}) - (3 - 4\nu')(A_{21} - \overline{A}_{21}) + 4(1 - \nu')(A_3 - \overline{A}_3) & \text{continuity of } u_3 \\ &= \frac{\mu'}{\mu''} \{A'_{11} - (3 - 4\nu'')A'_{21} + 4(1 - \nu'')A'_3\} & \text{continuity of } u_3 \\ (A_{12} + \overline{A}_{12}) - (3 - 4\nu')\overline{A}_{22} &= \frac{\mu'}{\mu''} \{A'_{12} - (3 - 4\nu'')A'_{22}\} & \text{continuity of } u_3 \\ (A_{11} - \overline{A}_{11}) - (1 - 2\nu')(A_{21} - \overline{A}_{21}) + 2(1 - \nu')(A_3 - \overline{A}_3) & \text{continuity of } \gamma_{31} \text{ and } \gamma_{32} \\ &= A'_{11} - (1 - 2\nu'')A'_{21} + 2(1 - \nu'')A'_3 & \text{continuity of } \gamma_{31} \text{ and } \gamma_{32} \\ (A_{12} + \overline{A}_{12}) - (1 - 2\nu')\overline{A}_{22} &= A'_{12} - (1 - 2\nu'')A'_{22} & \text{continuity of } \gamma_{31} \text{ and } \gamma_{32} \\ &= A'_{11} - 2(1 - \nu')(A_{21} + \overline{A}_{21}) + 2(1 - \nu')(A_3 + \overline{A}_3) & \text{continuity of } \sigma_{33} \\ &= A'_{11} - 2(1 - \nu'')A'_{21} + 2(1 - \nu'')A'_3 & \text{continuity of } \sigma_{33} \\ (A_{12} - \overline{A}_{12}) + 2(1 - \nu')\overline{A}_{22} &= A'_{12} - 2(1 - \nu'')A'_{22} & \text{continuity of } \sigma_{33} \end{cases}$$

Substituting Eqs. (11) and (13) into Eq. (15), eight coefficients $\overline{A}_{11} \cdots A'_{22}$ can be solved as Eq. (16),

$$\overline{A}_{11} = A_3 - 2\mu' \left[\frac{A_3'(1 - \nu'')}{(3 - 4\nu'')\mu' + \mu''} + \frac{(A_3 + \overline{A}_3)(1 - \nu')}{(3 - 4\nu')\mu'' + \mu'} \right]
\overline{A}_{12} = A_3 x_3' \frac{(3 - 4\nu')(\mu' - \mu'')}{(3 - 4\nu')\mu'' + \mu'}, \quad \overline{A}_{21} = \frac{4\overline{A}_3(1 - \nu')\mu'' - A_3(\mu' - \mu'')}{(3 - 4\nu')\mu'' + \mu'}
\overline{A}_{22} = 2A_3 x_3' \frac{\mu' - \mu''}{(3 - 4\nu')\mu'' + \mu'}, \quad A_{11}' = -2\mu'' \left[\frac{A_3'(1 - \nu'')}{(3 - 4\nu'')\mu' + \mu''} + \frac{(A_3 + \overline{A}_3)(1 - \nu')}{(3 - 4\nu')\mu'' + \mu'} \right]
A_{12}' = -4A_3 x_3' \frac{(1 - \nu')\mu''}{(3 - 4\nu')\mu'' + \mu'}, \quad A_{21}' = 4A_3' \frac{(1 - \nu'')\mu'}{(3 - 4\nu'')\mu' + \mu''}, \quad A_{22}' = 0$$
(16)

By using all coefficients, the bi-material thermoelastic solution can be simplified as,

(a) When $x_3'x_3 \ge 0$, the source and field points are in the same material phase,

$$2\mu' u_{i}(\mathbf{x}) = A_{3}\psi_{,i} + \overline{A}_{11}\overline{\beta}_{,i}^{u} + (\overline{A}_{12} + x_{3}\overline{A}_{21})\overline{\alpha}_{,i}^{u} + x_{3}\overline{A}_{22}\overline{\phi}_{,i} + \delta_{i3} \left[-(3 - 4v')(\overline{A}_{21}\overline{\alpha}^{u} + \overline{A}_{22}\overline{\phi}) + 4(1 - v')\overline{A}_{3}\overline{\alpha}^{u} \right]$$
(17)

(b) When $x_3'x_3 < 0$, the source and field points are in different material phases,

$$2\mu''u_i(\mathbf{x}) = A'_{11}\beta_{,i}^{u'} + A'_{12}\alpha_{,i}^{u'} + x_3(A'_{21}\alpha_{,i}^{u'} + A'_{22}\phi_{,i}) + \delta_{i3}\alpha^{u'} \left[-(3 - 4\nu'')A'_{21} + 4(1 - \nu'')A'_3 \right]$$

$$(18)$$

where the $\alpha^{u'}$ and $\beta^{u'}$ potential functions are canceled in Eq. (17) as no discontinuity is allowed by the sign function when $x_3 = x_3'$; in Eq. (18), because the source point is located at the upper phase, $S(x_3 - x_3') = -1$, therefore, $\beta^{u'} = \beta^u$ and $\alpha^{u'} = -\alpha^u$ can be obtained.

The present form of bi-material thermoelastic fundamental solution can be used to investigate induced elastic fields caused by heat sources at any arbitrary interior point. Its application to Eshelby's problem is, however, complicated due to the domain integral on x'_3 . Hence, in the following subsection, the bi-material thermoelastic fundamental solution will be modified to get rid of free source x'_3 terms of the coefficients \overline{A}_{12} , \overline{A}_{22} and A'_{12} .

3.3. Modified bi-material thermoelastic fundamental solution

It is possible to rewrite distance components in terms of $\mathbf{r} = \mathbf{x} - \mathbf{x}'$ so that \mathbf{x}' can be replaced by $\mathbf{x}' = \mathbf{x} - \mathbf{r}$ (Wu et al., 2021b). By virtue of Galerkin's distance vector, this subsection aims to remove any free x_3' of the coefficients, i.e \overline{A}_{12} , \overline{A}_{22} and A_{12}' , which simplifies the domain integral expressions.

(a) When $x_3'x_3 \ge 0$, the source and field points are in the same material phase. The coefficients \overline{A}_{12} and \overline{A}_{22} contains x_3' , and their related potential functions can be altered as below,

$$2\mu' u_{i}(\mathbf{x}) = A_{3}\psi_{,i} + (\overline{A}_{11} + L_{D}^{u})\overline{\beta}_{,i}^{u} + L_{B}^{u}\overline{\psi}_{,i} + x_{3} \left[(L_{D}^{u} - L_{F}^{u})\overline{\alpha}_{,i}^{u} + L_{C}^{u}(\overline{\psi}_{,i3} + 2(1 - 2\nu')\delta_{i3}\overline{\phi} - x_{3}\overline{\phi}_{,i}) \right] + \delta_{i3} \left[-(3 - 4\nu')(\overline{A}_{21}\overline{\alpha}^{u} + L_{C}^{u}\overline{\psi}_{,3}) + (4(1 - \nu')\overline{A}_{3} - L_{B}^{u})\overline{\alpha}^{u} \right]$$
(19)

where the coefficients L_{R}^{u} , L_{C}^{u} , L_{D}^{u} and L_{E}^{u} are,

$$L_{B}^{u} = A_{3} \frac{(3 - 4v')(\mu' - \mu'')}{(3 - 4v')\mu'' + \mu'}, \quad L_{C}^{u} = 2A_{3} \frac{(\mu' - \mu'')}{(3 - 4v')\mu'' + \mu'}$$

$$L_{D}^{u} = \frac{4\overline{A_{3}}(1 - v')\mu''}{(3 - 4v')\mu'' + \mu'}, \quad L_{F}^{u} = \frac{4A_{3}(\mu' - \mu'')(1 - v')}{(3 - 4v')\mu'' + \mu'}$$
(20)

(b) When $x'_3x_3 < 0$, the source and field points are in different material phases. The coefficient A'_{12} contains x'_3 , and its related components have been revised as below,

$$2\mu''u_i(\mathbf{x}) = (A'_{11} + L_G^u)\beta_{,i}^u - x_3 \left[A'_{21} - L_G^u \right] \alpha_{,i}^u + L_G^u \psi_{,i} - \delta_{i3}\alpha^u \left[-L_G^u - (3 - 4\nu'')A'_{21} + 4(1 - \nu'')A'_3 \right]$$
(21)

where the coefficient $L_G^u = \frac{4A_3(1-v')\mu''}{(3-4v')\mu''+\mu'}$. The derivation of fundamental solution for $x_3' < 0$ is similar to Section 3.2. Alternatively, one can acquire the solution by switching the material constants and the sign of coordinates. For example, two cases that (i) $u_i(\mathbf{x})$ caused by the heat source at \mathbf{x}' ; (ii) $u_i(-\mathbf{x})$ caused by the heat source at $-\mathbf{x}'$ shall share the same form of the solution with the alternative material constants. Hence, the complete form of the thermoelastic Green's function is written as,

$$2\mu^{q}G_{i}(\mathbf{x}, \mathbf{x}') = \begin{cases} A_{3}^{q}\psi_{,i} + (\overline{A}_{11}^{q} + L_{B}^{y})\overline{\beta}_{,i}^{y} + L_{B}^{y}\overline{\psi}_{,i} \\ + x_{3} \left[\chi \left(L_{D}^{y} - L_{F}^{y} \right)\overline{\alpha}_{,i}^{y} + L_{C}^{y} (\overline{\psi}_{,i3} + 2(1 - 2v^{q})\delta_{i3}\overline{\phi} - x_{3}\overline{\phi}_{,i}) \right] & x_{3}x_{3}' \ge 0 \\ + \delta_{i3} \left[-(3 - 4v^{q})(\overline{A}_{21}^{q}\overline{\alpha}^{y} + L_{C}^{y}\overline{\psi}_{,3}) + \chi \left(4(1 - v^{q})\overline{A}_{3}^{q} - L_{B}^{y} \right)\overline{\alpha}^{y} \right] \\ (A_{11}^{q'} + L_{G}^{y})\beta_{,i}^{y} - x_{3} \left[A_{21}^{q'} - L_{G}^{y} \right]\alpha_{,i}^{y} + L_{G}^{y}\psi_{,i} \\ - \chi \delta_{i3}\alpha^{l} \left[L_{G}^{y} + (3 - 4v^{q})A_{3}^{q'} - 4(1 - v^{q})A_{3}^{q'} \right] \end{cases}$$
 $x_{3}x_{3}' < 0$

where the superscript q indicates two cases: q=' when $x_3 \ge 0$ and q='' when $x_3 < 0$; the superscript y and coefficient χ are defined in Eq. (3) that y=', $\chi=1$ when $x_3' \ge 0$ and y='', $\chi=-1$ when $x_3' < 0$; similarly to coefficients A^l-G^l the coefficients $L_B^l-L_G^l$ can be obtained through switching the material sequence in Eq. (20).

When one material phase is reduced to a vacuum with K' = C' = 0, the infinite bi-material is reduced to a semi-infinite single material domain with a free boundary condition from heat flux and traction along the surface. The corresponding Green's function can be obtained from the above fundamental solution, and explicitly written in Eqs. (B.1)–(B.3) of Appendix B. On the other hand, When one material phase is reduced to an ideally rigid thermal conductor with $K' \to \infty$, A = 0, and $C' \to \infty$, the infinite bi-material is reduced to a semi-infinite single material domain exhibiting a boundary condition with a fixed uniform temperature and displacement along the surface. Particularly, when the two phases exhibit the same material properties, the thermoelastic Green's function reduces to the one for a single material domain. The corresponding Green's functions are given Appendix B.

Using Hadamard's regularization, the two-dimensional (2D) biharmonic potential ψ^{2D} can be obtained. Following the same fashion, through the partial integration along the second axis, the two-dimensional Boussinesq's displacement potentials can be derived and substituted into Eq. (22), and the explicit forms are available in Chapter 2 of the book (Yin et al., 2022). Therefore, the present 3D formulation can be rewritten in the 2D case as well.

3.4. The dual equivalent inclusion method (DEIM)

When an infinite space contains an inhomogeneity, Eshelby (1957, 1959) proposed to replace the inhomogeneity with an inclusion with a uniformly distributed eigenstrain, where the disturbed elastic fields are calculated through the domain integral of the modified Green's function over the inclusion, namely the Eshelby's tensor. Following the same fashion (Hatta and Taya, 1986; Wang et al., 2022), the EIM has been extended for heat conduction in full space and bi-materials. Based on the merits of Green's function, it provides the particular solution due to one unit excitation at a source point, which can either be a heat source

or force. Thermoelastic Green's function provides the displacement field caused by a point heat source. The temperature fields have been solved recently with the Green's function in Wang et al. (2022). However, the three Green's functions are only applicable to the infinite bi-material domain without any inhomogeneity. Because the present inhomogeneity exhibits different thermal conductivity, thermal expansion coefficient, and stiffness, Eshelby's equivalent inclusion method cannot be directly applied (Eshelby, 1957, 1959) to thermal stress analysis due to the temperature variation and material inhomogeneity, which produces coupled effect to thermal stress. If the thermal stress is simulated in a decoupled way with the temperature field and then the displacement field, it is doable but the calculation will be complicated as the temperature changes over the whole domain. The DEIM is introduced to simulate the effect of material mismatch by an eigenstrain and ETG over the inclusion, so that the displacement field can be obtained by the integral over the inclusion only.

3.4.1. One inclusion in two-jointed half-spaces

First, we assume the subdomain Ω^I exhibits the same material properties as the matrix, the displacement caused by eigenstrain and ETG can be obtained by the integral of the Green's function on these source fields on the subdomain, which is called inclusion instead of inhomogeneity (Mura, 1987). Due to the disturbance of boundary effects and inhomogeneity interactions, which will be elaborated later, both the eigen-temperature gradient $T_i^*(\mathbf{x})$ and eigenstrain $\varepsilon_{ij}^*(\mathbf{x})$ are given in a polynomial form referred to the center of the Ith subdomain Ω^I to represent the varying eigen-fields as,

$$\varepsilon_{ij}^{*}(\mathbf{x}) = \varepsilon_{ij}^{I0*} + (x_{p} - x_{p}^{Ic})\varepsilon_{ijp}^{I1*} + (x_{p} - x_{p}^{Ic})(x_{q} - x_{q}^{Ic})\varepsilon_{ijpq}^{I2*} + \cdots
T_{i}^{*}(\mathbf{x}) = T_{i}^{I0*} + (x_{k} - x_{k}^{Ic})T_{i}^{I1*} + (x_{k} - x_{k}^{Ic})(x_{l} - x_{l}^{Ic})T_{ikl}^{I2*} + \cdots$$
(23)

where \mathbf{x}^{Ic} is the center of Ω^I as shown in Fig. 2; and ε^{I0*}_{ij} , ε^{I1*}_{ijp} , ε^{I2*}_{ijp} and T^{I0*}_i , T^{I1*}_{ik} , T^{I2*}_{ikl} are uniform, linear and quadratic components of polynomial to approximate the eigenstrain and eigen-temperature-gradient in the Ith inhomogeneity, respectively. Using the Green's function in Eqs. (4) and (22), the induced displacement field can be acquired through Gauss' theorem (Mura, 1987) as below,

$$u_{i}(\mathbf{x}) = \int_{\Omega_{I}} \frac{\partial G_{ij}(\mathbf{x}, \mathbf{x}')}{\partial x'_{m}} \varepsilon_{kl}^{*}(\mathbf{x}') C_{jmkl}(\mathbf{x}') dV(\mathbf{x}') + \int_{\Omega_{I}} \frac{\partial G_{i}(\mathbf{x}, \mathbf{x}')}{\partial x'_{k}} T_{k}^{*}(\mathbf{x}') K(\mathbf{x}') dV(\mathbf{x}')$$

$$= g_{ikl} \varepsilon_{kl}^{I0*} + g_{iklp} \varepsilon_{kl}^{I1*} + g_{iklpq} \varepsilon_{klpq}^{I2*} + W_{ik} T_{k}^{I0*} + W_{ikp} T_{kp}^{I1*} + W_{ikpq} T_{kpq}^{I2*}$$
(24)

where $g_{iklpq} = \int_{\Omega} G_{ij,m'} C_{jmkl}(x_p - x_p^{Ic})(x_q - x_q^{Ic}) dV(\mathbf{x}')$ and $W_{ikpq} = \int_{\Omega} G_{i,k'} K(x_p - x_p^{Ic})(x_q - x_q^{Ic}) dV(\mathbf{x}')$ are Eshelby's tensors relating eigenstrain and eigen-temperature-gradient to displacement field, respectively; g_{iklp} , g_{ikl} , W_{ikp} and W_{ik} are defined in the similar fashion; $G_{ij}(\mathbf{x},\mathbf{x}')$ and $G_i(\mathbf{x},\mathbf{x}')$ are the elastic and thermoelastic Green's functions given in Eqs. (4) and (22), respectively. Using the compatibility relationship, the mechanical strain at interior point \mathbf{x} can be derived,

$$\varepsilon_{ij}^{m}(\mathbf{x}) = \varepsilon_{ij}^{\prime}(\mathbf{x}) + \varepsilon_{ij}^{H}(\mathbf{x}) - \alpha \Delta T(\mathbf{x}) \delta_{ij} = \left[S_{ijkl} \varepsilon_{kl}^{I0*} + S_{ijklp} \varepsilon_{klp}^{I1*} + S_{ijklpq} \varepsilon_{klpq}^{I2*} \right] \\
+ \left[R_{ijk} T_{k}^{I0*} + R_{ijkp} T_{kp}^{I1*} + R_{ijkpq} T_{kpq}^{I2*} \right] - \alpha \delta_{ij} \left[D_{k} T_{k}^{I0*} + D_{kp} T_{kp}^{I1*} + D_{kpq} T_{kpq}^{I2*} \right]$$
(25)

where $S_{ijklpq} = \frac{g_{iklpq,j} + g_{jklpq,i}}{2}$ and $R_{ijkpq} = \frac{W_{ikpq,j} + W_{jkpq,i}}{2}$ are Eshelby's tensor for strain; $D_{kpq} = \int_{\Omega} G_{,k'} K(\mathbf{x}') (x_p - x_p^{Ic}) (x_q - x_q^{Ic}) dV(\mathbf{x}')$ is the Eshelby's tensor relating eigen-temperature gradient to temperature; and $S_{iklp}, S_{ikl}, R_{ijkp}, R_{ijk}, D_{kp}$, and D_k are defined in the similar fashion.

Notice that in micromechanics, the thermal strain caused by the temperature variation is typically considered as an eigenstrain directly. There is a misconception that the ETG will produce a temperature change over the whole domain that yields an eigenstrain over the whole domain, which makes the thermoelastic solution inefficient. The thermoelastic Green's function handles the strain caused by ETG directly with R tensors instead of an eigenstrain with S tensors in Eq. (25), therefore, the volume integral is still limited to the inclusion, which can be analytically solved.

3.4.2. One inhomogeneity in two-jointed half-spaces D

In the previous subsection, the induced elastic fields by the polynomial-form eigenstrain and ETG can be obtained through the domain integral of three Green's functions over the subdomain. Unlike the inclusion problems, the subdomain is filled with another material with stiffness C^I , thermal conductivity K^I and thermal modulus \mathcal{A}^I . The polynomial-form equivalent flux conditions are presented for the uniform, linear and quadratic ETGs as below (Yin et al., 2022),

$$K^{w}(T_{i}^{\infty} + T_{i}' + T_{i}^{Q} - T_{i}^{I0*}) = K^{I}(T_{i}^{\infty} + T_{i}' + T_{i}^{Q})$$

$$K^{w}(T_{i,m}^{\infty} + T_{i,m}' + T_{i,m}^{Q} - T_{im}^{I1*}) = K^{I}(T_{i,m}^{\infty} + T_{i,m}' + T_{i,m}^{Q})$$

$$K^{w}(T_{i,mn}^{\infty} + T_{i,mn}' + T_{i,mn}^{Q} - 2T_{imn}^{I2*}) = K^{I}(T_{i,mn}^{\infty} + T_{i,mn}' + T_{i,mn}^{Q})$$
(26)

where w is dependent on the position of the subdomain Ω^I that when $x_3' > 0$ w = ', and otherwise w = ''; T_i^{∞} is the far-field prescribed temperature gradient; T_i' and T_i^Q are disturbed temperature gradient by ETG and prescribed heat source, respectively. Subsequently, the stress equivalent conditions can be constructed for the uniform, linear, and quadratic eigenstrain as,

$$C_{ijkl}^{w}(\varepsilon_{kl}^{\infty} + \varepsilon_{kl}^{\prime} + \varepsilon_{kl}^{Q} + \varepsilon_{kl}^{E} - \varepsilon_{kl}^{I0*}) - \mathcal{A}^{w}\delta_{ij}\Delta T = C_{ijkl}^{I}(\varepsilon_{kl}^{\infty} + \varepsilon_{kl}^{\prime} + \varepsilon_{kl}^{Q} + \varepsilon_{kl}^{E}) - \mathcal{A}^{I}\delta_{ij}\Delta T$$

$$C_{ijkl}^{w}(\varepsilon_{kl,m}^{\infty} + \varepsilon_{kl,m}^{\prime} + \varepsilon_{kl,m}^{Q} + \varepsilon_{kl,m}^{E} - \varepsilon_{klm}^{I1*}) - \mathcal{A}^{w}\delta_{ij}\Delta T_{,m} = C_{ijkl}^{I}(\varepsilon_{kl}^{\infty} + \varepsilon_{kl}^{\prime} + \varepsilon_{kl}^{Q} + \varepsilon_{kl}^{E})_{,m} - \mathcal{A}^{I}\delta_{ij}\Delta T_{,m}$$

$$C_{ijkl}^{w}(\varepsilon_{kl,mn}^{\infty} + \varepsilon_{kl,mn}^{\prime} + \varepsilon_{kl,mn}^{Q} + \varepsilon_{kl,mn}^{E} - 2\varepsilon_{klmn}^{I2*}) - \mathcal{A}^{w}\delta_{ij}\Delta T_{,mn} = C_{ijkl}^{I}(\varepsilon_{kl}^{\infty} + \varepsilon_{kl}^{\prime} + \varepsilon_{kl}^{Q} + \varepsilon_{kl}^{E})_{,mn} - \mathcal{A}^{I}\delta_{ij}\Delta T_{,mn}$$

$$(27)$$

where ϵ_{ij}^{∞} represents the far-field prescribed strain; ϵ_{ij}' can calculated through Eq. (25) with the polynomial-form eigenstrain ϵ_{ij}^{I*} ; ϵ_{ij}^{Q} and ϵ_{ij}^{E} are disturbed strain field caused by heat source and ETG, respectively; $\mathcal{A}\delta_{ij}\Delta T$ is non-mechanical stress caused by temperature change. Furthermore, the equivalent conditions can be extended to multiple subdomains through the superposition of disturbed strain caused by eigenstrain, heat source and ETGs, which is illustrated in Section 5 with the case studies of several spherical heat exchangers. The dual equivalent inclusion method (DEIM) separates the coupled thermoelastic problem in two sets of Eqs. (26) and (27), however, they can be straightforwardly combined into one global matrix for the numerical solution.

As mentioned in the previous subsection, the eigen-fields are expanded at the center of the inhomogeneity due to boundary and interaction effects. The term, boundary effect, is first mentioned when the field point is close to the boundary, where strong constraints may apply, resulting in a large variation of stress/thermal fields. As for a bi-layered system, since the two matrix materials generally exhibit dissimilar properties, such boundary (or interfacial) effect causes discontinuity of some stress components and significantly changes the slope of continuous stress (σ_{33} , τ_{13}), leading to large stress variations. The boundary (interfacial) effects are mathematically considered by the bi-material fundamental solutions, which hold certain continuity equations on thermal and stress fields. As for the inhomogeneity interactions, such effect becomes dominant when two inhomogeneities are close, and it usually causes disturbance of fields, such as higher-order stress variation, etc. Hence, indicated as Eq. (23), polynomial-form eigen-fields are applied. And the extension from one inhomogeneity to multiple inhomogeneities is elaborated in Section 1.3 of the Supplemental Material.

4. Numerical verification of the DEIM in a two-jointed half-spaces

This section aims to verify the algorithm of DEIM and demonstrate how solutions with uniform, linear and quadratic order polynomial-form eigen-fields perform. Notice that the order of eigen-fields applies to both ETG and eigenstrain at the same time. As introduced in Section 2, the boundary effects of bi-material interfaces and interactions between inhomogeneities significantly disturb the elastic and thermal fields, therefore Eshelby's solution with uniform eigenstrain cannot provide accurate predictions. In Eqs. (4) and (22), when the source and field points are in the same material phase, there exist image terms i.e $\overline{\psi}$, which results in the boundary or interfacial effects. Although the image terms vanish rapidly with increasing distance, the effects from eigen-fields depend on domain integrals. Therefore, for spherical subdomains, the interfacial effects are determined by the ratio h/a, where h and a are perpendicular distances of \mathbf{x}^{IC} , bi-material interface S and radius of the subdomain, respectively. Particularly, when the inhomogeneity is far from the bi-material interface, say $h/a \geq 5$, the interfacial effects become minor and the solutions are similar to infinite ones. Without the loss of any generality, the verification is conducted in a two-jointed half-spaces that the material properties of two layers and the inhomogeneity are, (i) $\mu' = 0.4$ MPa, $\nu' = 0.25$, K' = 1 W/(m K) and A' = 10 kPa for D^+ ; (ii) $\mu'' = 0.8$ MPa, $\nu' = 0.1$, $\nu' = 0.1$ MPa, $\nu' = 0.1$ MPa, $\nu' = 0.25$, $\nu' = 0.1$ MPa, $\nu' = 0.1$

4.1. Handling and transformation of domain integrals

Although the verification can be conducted with an infinite domain, to account for the influence of temperature change and compare with the finite element results, domain integrals cannot be avoided. Alternatively, shown as Fig. 3, consider a horizontally infinite space with height 2l at 2 m, where the bi-material interface S is placed at the center of D. Since, the calculation of temperature, displacement, and stress fields require references, without the loss of any generality, let the $T_2 = 0$ °C and $U_3 = 0$ be references. On the top surface, apply temperature load $U_1 = 100$ °C and uniformly distributed stress $U_3 = -10$ kPa. Therefore, the temperature difference between U_1 and U_2 produces a piece-wise continuous heat flux along the U_3 direction.

The domain integrals can be analytically handled through the application of Green's second identity. Although the authors (Prasad et al., 1994) present a dual boundary element method for the full-space thermoelastic problem, following the same fashion, it can be extended to the bi-material space by adjusting the thermoelastic Green's function. For a horizontally infinite space, because the influence of Green's function vanishes as $1/r^2$ and $1/r^3$ for displacement (temperature) and stress (flux) respectively, it is natural to consider a cut-off block with 10a width and length. Since the disturbance by inhomogeneity on the boundary is negligible, the interior thermoelastic displacement can be written in terms of surface integral only,

$$u_i^T(\mathbf{x}) = \int_{\partial O} G_i(\mathbf{x}, \mathbf{x}') q(\mathbf{x}') - G_{i,j'}(\mathbf{x}, \mathbf{x}) n_j(\mathbf{x}') K(\mathbf{x}') T(\mathbf{x}') dS(\mathbf{x}')$$
(28)

where q and T are prescribed outward flux and temperature on the six surfaces of the cut-off block; \mathbf{n} is the unit surface outward normal; $G_i(\mathbf{x}, \mathbf{x}')$ is the thermoelastic Green's function defined in Eq. (22). Similarly, the elastic parts can be calculated referring to Wu et al. (2022) and Yin et al. (2022). Notice that since the temperature distribution is linear, heat flux is zero on side surfaces, and constant on bottom and top surfaces, the domain integral can also be conducted in a simplified form referring to Gao (2003).

4.2. Comparison with the FEM results

Consider an inhomogeneity Ω^I is placed along the vertical center line with distance h/a = 1.5 in the upper phase \mathcal{D}^+ . The dimensions and boundary conditions are built upon Fig. 3. Three element sizes are applied, (i) 0.04 m for the matrix; (ii) 0.02 m for the transition zone $(0.3 \times 0.3 \times 0.3 \text{ m}^3)$; and (iii) 0.005 m for the inhomogeneity. 3,331,649 nodes and 2,453,741 10-node tetrahedral elements. Indicated in Fig. 4, the temperature and heat flux are compared between FEM and DEIM with uniform, linear and quadratic

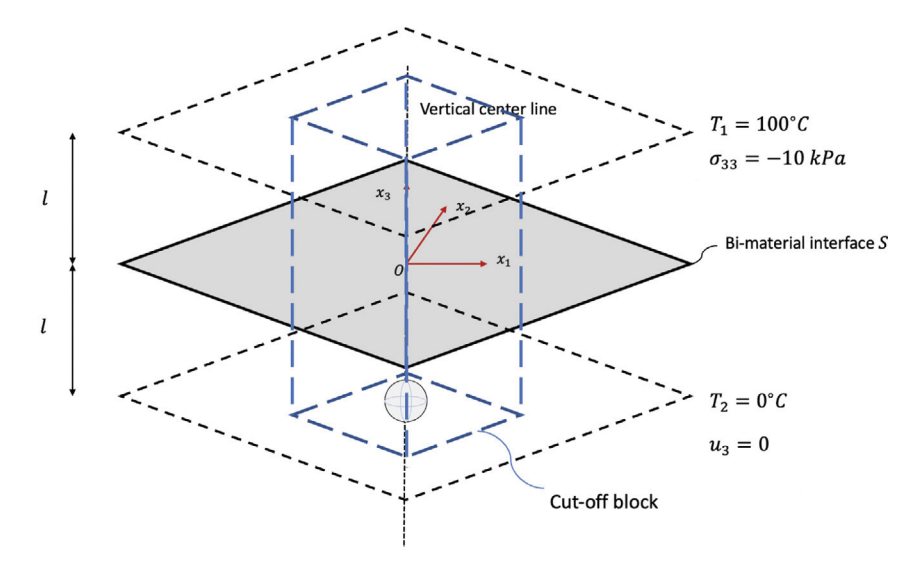


Fig. 3. Schematic illustration of the case study on a horizontally infinite large space with limited height 2l = 2m embedded with one inhomogeneity along the vertical center line, where temperature loads, stress loads and reference vertical displacement and temperature are prescribed with a cut-off block.

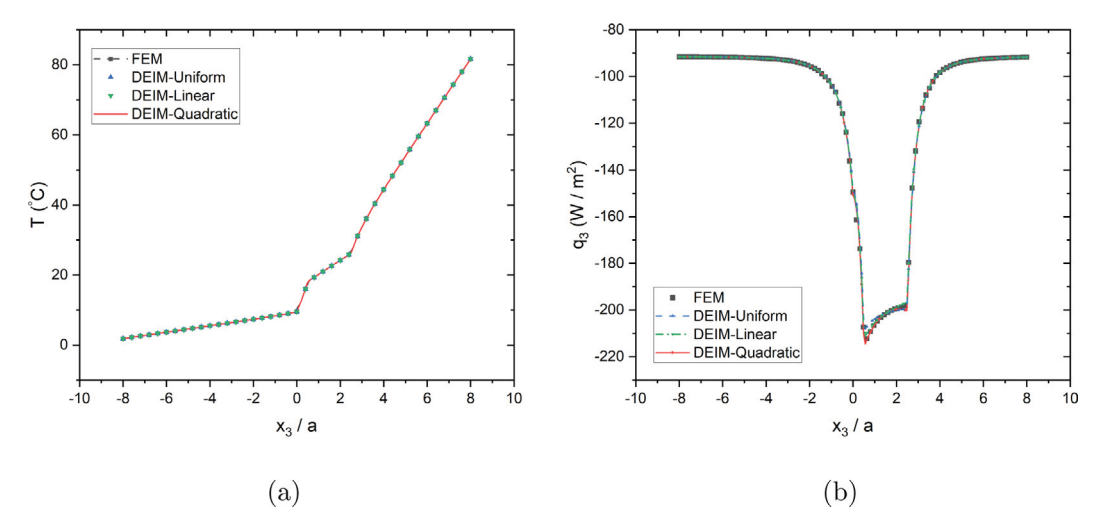


Fig. 4. Comparison of DEIM with three orders of polynomial ETG with FEM on (a) temperature T (b) heat flux q_3 along the vertical center line when distance ratio h/a = 1.5.

orders of ETG. Despite that some errors may arise with assumptions of no boundary interactions, the comparison of temperature curves exhibits good agreement among all orders of ETG as very minor discrepancies are observed. However, as shown in Fig. 4(b), merely constant eigen-fields may not be suitable to provide accurate predictions on a higher order field, i.e the heat flux. In addition, the two curves "DEIM - Linear" and "DEIM - Quadratic" exhibit close predictions, and the main discrepancy exists at the entering region of the inhomogeneity ($x_3 = 0.05$), which is due to the bi-material interfacial effects.

The greater variance in ETG and its subsequent domain integrals result in larger fluctuations. Therefore, the larger differences among thermoelastic solutions with uniform, linear and quadratic eigen-fields are accumulated errors, which can be shown that in Fig. 4(b) the discrepancy for heat flux is much smaller than those in Fig. 6(b). Note that σ_{33} is continuous in the x_3 direction, so the curves in Fig. 6(b) are more consistent with each other in comparison with Fig. 6(a).

Considering the potentially larger numerical errors in DEIM with uniform and linear eigen-fields, thus in the following, merely quadratic eigen-fields are applied. In general, interfacial effects are more intensive with smaller distance ratios h/a. In this section, 4 cases of distance ratios h/a = 1.2, 1.5, 2.0, and 3.0 are considered, where the material properties and assumptions are retained from the previous section. The temperature and displacement in general show better comparison than the heat flux or stress shown in Figs. 4(a) and 5 in the last subsection. Here one can find a similar trend that DEIM fits excellently with the FEM results in Figs. 7(a) and 8.

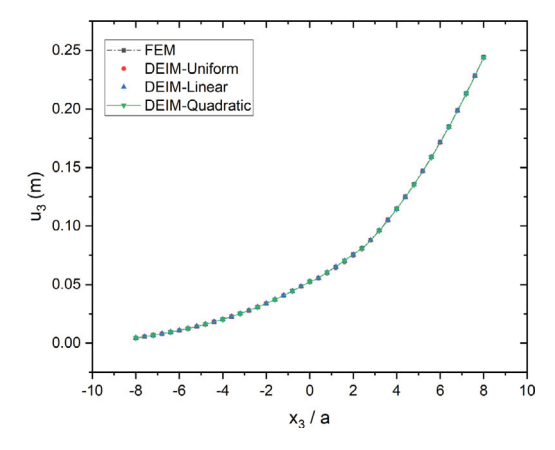


Fig. 5. Comparison of DEIM with three orders of polynomial ETG and eigenstrain with FEM on displacement u_3 along the vertical center line when distance ratio h/a = 1.5.

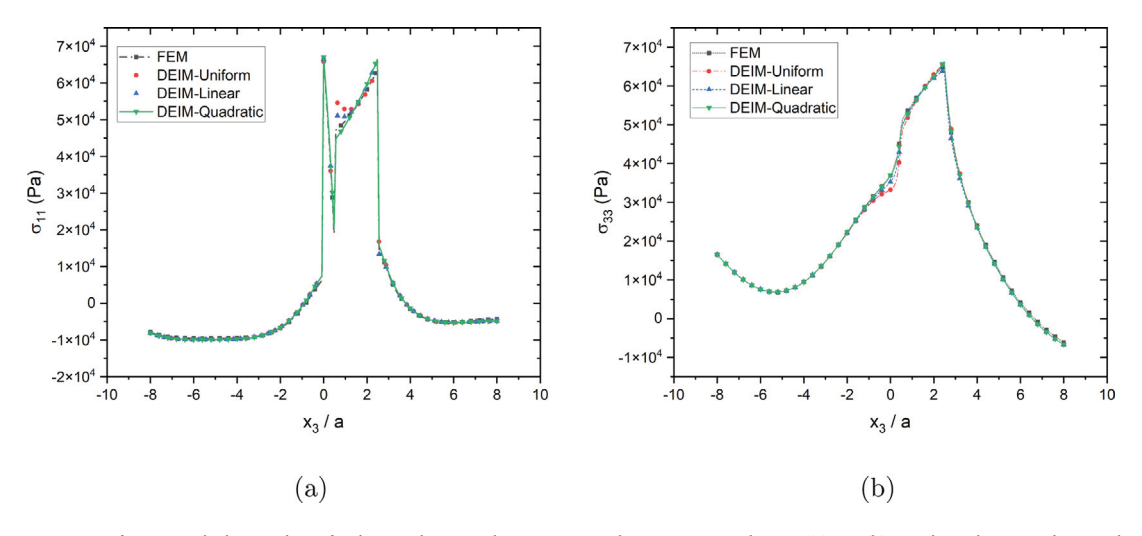


Fig. 6. Comparison of DEIM with three orders of polynomial ETG and eigenstrain with FEM on normal stress (a) σ_{11} (b) σ_{33} along the vertical center line when distance ratio h/a=1.5.

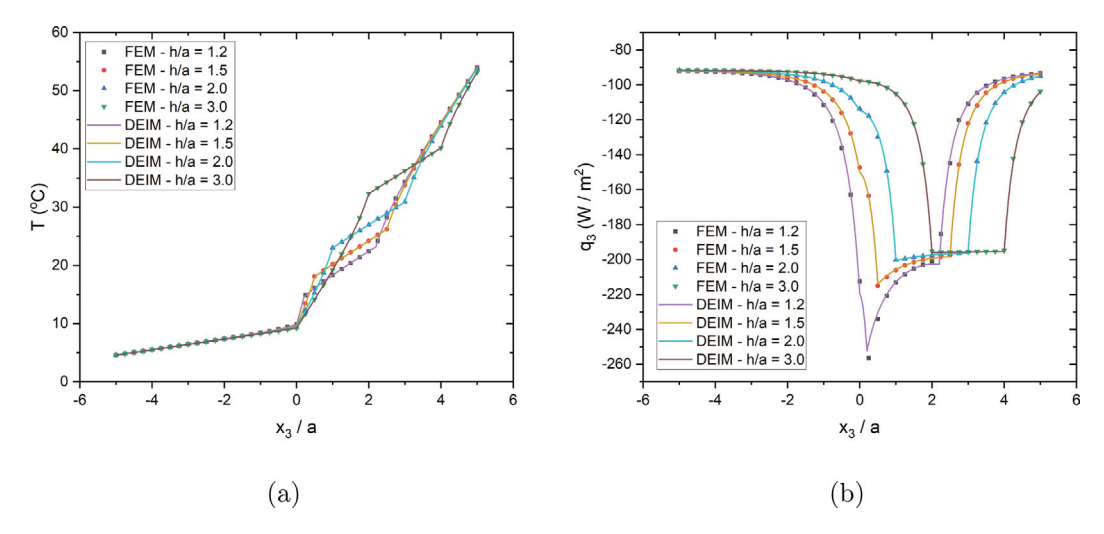


Fig. 7. Comparison of DEIM with quadratic ETG with FEM on (a) temperature T (b) heat flux q_3 along the vertical center line $x_3 \in [-5a, 5a]$ when distance ratios h/a = 1.2, 1.5, 2.0 and 3.0.

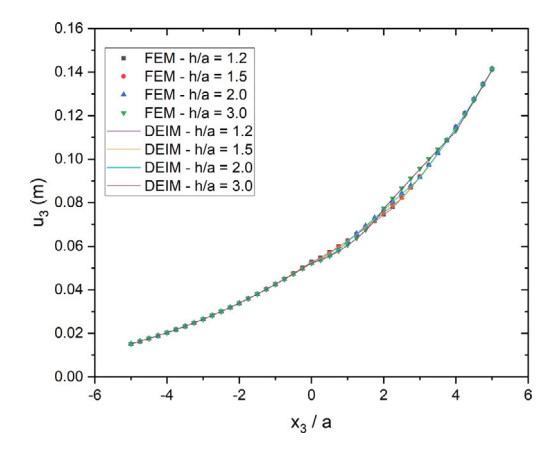


Fig. 8. Comparison of DEIM with quadratic ETG and eigenstrain with FEM on displacement u_3 along the vertical center line $x_3 \in [-5a, 5a]$ when distance ratios h/a = 1.2, 1.5, 2.0 and 3.0.

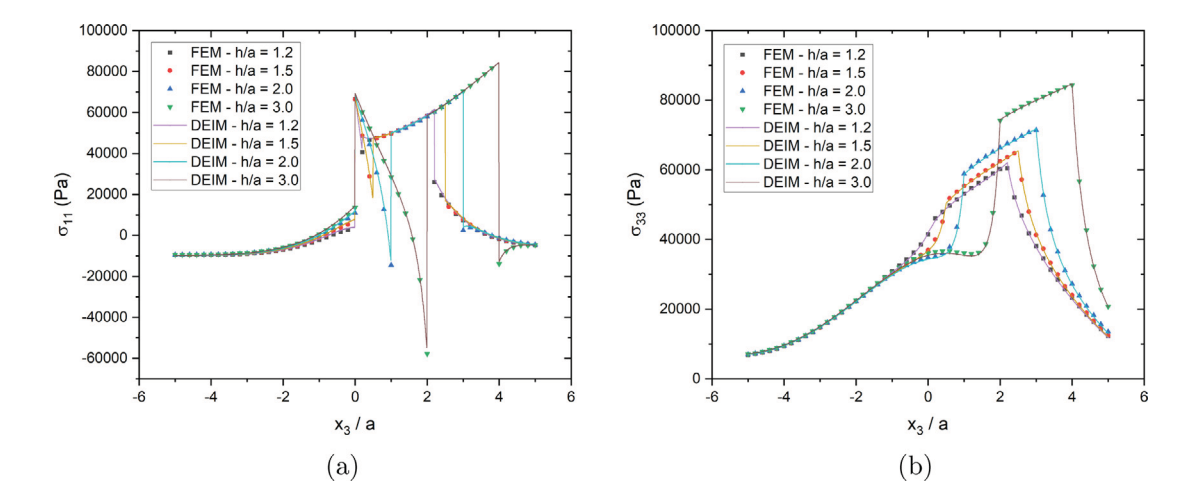


Fig. 9. Comparison of DEIM with quadratic ETG and eigenstrain with FEM on normal stress (a) σ_{11} (b) σ_{33} along the vertical center line $x_3 \in [-5a, 5a]$ when distance ratio h/a = 1.2, 1.5, 2.0 and 3.0.

Indicated in Figs. 3–5, the influence brought by the inhomogeneity and its eigen-fields vanishes rapidly with further observing distances. Hence, the thermal and elastic fields are compared in a range of 5a around the bi-material interface S as $x_3 \in [-5a, 5a]$. Indicated in Fig. 7(a), interfacial effects change the slope of temperature curves in the neighborhood of the inhomogeneity. When the distance ratio h/a decreases, the variation of temperature increases, which results in a larger heat flux at the bottom of the inhomogeneity. In Fig. 7, there exists 18% difference of heat flux q_3 between curve h/a = 1.2 and h/a = 1.5 when $x_3 = 0.02$ m. Because the elastic fields are dependent on thermal loads, the accumulated interfacial effects cause larger stress variations than a pure elastic problem. Shown in Fig. 9(a), one typical example on interfacial effects, it is observed that narrower stress difference at the interface $x_3 = 0.02$ (bottom of the inhomogeneity) with smaller distance ratios. Comparing two cases with distance ratios 1.2 and 3, the jump of normal stress σ_{11} increases approximately 14 times and similar trends exist for comparison of σ_{33} . Such phenomenon can be interpreted as a weakly interfacial "constraint", because the lower phase D^- is filled with stiffer material. When the distance ratio increases, the interfacial effects vanish almost one time faster than 1/r for displacement and temperature, since the distance to interface with image terms is generally doubled. As a limiting and ideal case, when the inhomogeneity is adequate far from the bi-material interface, the solution process reduces to the superposition of Kelvin's solution of concentrated force and Nowacki's solution of thermoelasticity, which will be further discussed in the last section.

More comparisons between the DEIM and FEM results for one and two inhomogeneities in a bi-material are provided in Section 1 of the Supplemental Material. The DEIM provides excellent agreement with the FEM results with quadratic eigenfields for all cases. Note that FEM has been computationally expensive to get convergent results for the infinite bi-material domain; whereas DEIM is straightforward. It has great potential to be used for the design and analysis of future geothermal systems.

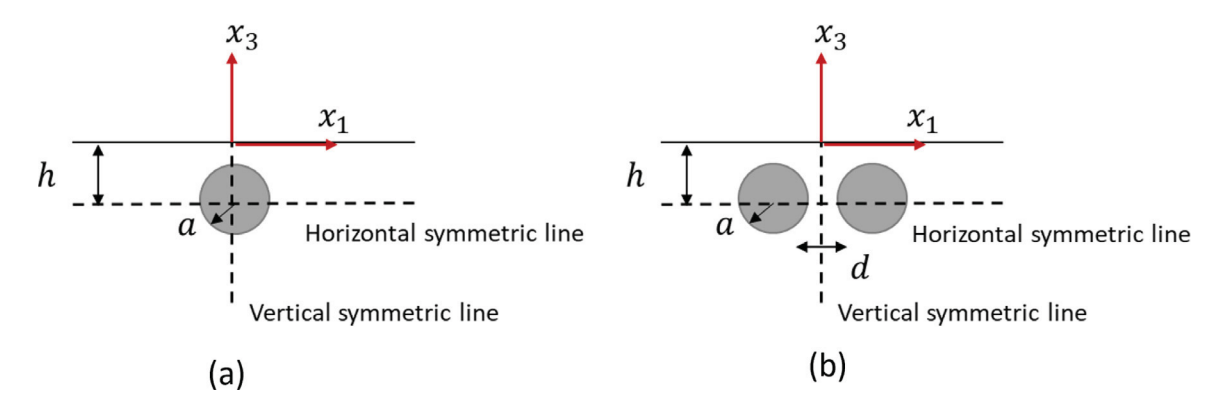


Fig. 10. Schematic illustration of (a) one inhomogeneity and (b) two inhomogeneities embedded at depth h with distance d and vertical, horizontal symmetric lines.

5. Application to geothermal systems with spherical tanks

Section 4 verifies the DEIM for a bi-material space with a heat source on a spherical heat exchanger. The method can be modified for geothermal applications with a spherical thermal tank at a certain depth h to the surface. For simplicity, the heat exchanger is assumed to be a homogeneous solid sphere although it is a spherical container filled with thermal fluid, such as water. The hydrodynamic behavior of water may significantly change the heat transfer process and local temperature field with both mass and heat transfer depending on time and space. Since this work focuses on the demonstration and applications of the present algorithm with formulations, an actual tank is simplified into a uniform solid sphere. Using the multi-inclusion model by Hori and Nemat-Nasser (1993) and Herve (2002), the spherical tank indeed can be approximated into a homogeneous sphere with the formulation provided in Appendix C for future field validation. In addition, soils generally exhibit viscoelastoplastic behavior, which depends on loading rate and history, with complicated constitutive relations. However, this paper still focuses on the elastic analysis as a baseline for future case studies with field test data and material characterization. In this section, three aspects are considered, (i) stress transfer caused by surface loads; (ii) thermal stresses caused by the heat source; and (iii) thermoelastic fields by multiple heat exchangers. In the following, the effects of depth h, stiffness \mathcal{C}^I are discussed. Let the soil be unsaturated clay and its Young's modulus and Poisson's ratio are 20 MPa and 0.3, respectively; consider a free-surface at $x_3 = 0$, so that the stiffness \mathcal{C}^I is set as zero. In the following, the thermal and elastic fields are investigated along the two symmetric lines as shown in Fig. 10. When the depth h of a tank is large, it converges to the exact solution for a spherical inhomogeneity in an infinite domain with a single material.

5.1. The stress transfer from the surface to the tank

For an underground heat exchanger, the stress transfer can be caused by surface loads, such as nearby parked trucks, where the load transfer can be considered with a contact problem. However, the distance between the tire to the thermal tank should be much larger than the dimension of the tire contact area. Although a uniformly distributed load in a rectangular loading area may not be as accurate as that from the contact mechanics, the difference will be minimal. As an application case study, the parameters are set as, (i) the radius a = 1.5 m for the heat exchanger; (ii) the dimension of rectangle loading region is 1.5×3.75 m² and (iii) the load 10^5 N is uniformly distributed on the loading region as $\frac{160}{9}$ kPa downward pressure. Since the disturbance displacement and strain vanish rapidly with distance, only points in the range of [-4a, 4a] around the center of inhomogeneity are illustrated. Four depths, h = 5, 10, 15 and h = 20 a, are selected and to control other variables, the stiffness C^I equals 100C''. Fig. 11(a) exhibits the distribution of u_3 along the vertical symmetry line, and the variations narrow with increasing depth h, which can be interpreted as the influence of surface loads also vanishes rapidly with depth. Because the heat exchanger is much stiffer than neighbor soils, the variation of displacement within the exchanger is small. Similar trends can be observed in Figs. 11(b-d). Notice that because the surface is not axis-symmetric, σ_{11} and σ_{22} exhibits discrepancies for case h = 5a and such differences reduces for the other three curves.

To investigate the effects of stiffness ratios, six stiffness of the heat exchanger are considered as 0.1, 0.2, 0.5, 2, 5 and 20 C'' and the depth h is 10a. Fig. 12(a) exhibits the distribution of u_3 along the vertical symmetric line that variations of displacement within the inhomogeneity become narrower with larger stiffness ratios. The disturbance of eigen-fields is approximately limited in the range of [-3,3]a as minor discrepancies are observed beyond the range. Fig. 12(b) and (c) plots the variation of normal stress σ_{11} and σ_{22} , because of the depth h = 10a, the differences between σ_{11} and σ_{22} of the same case are negligible. When the exchanger is softer, although the slope of displacement increases, the stress generally is smaller. However, the stress concentrations by discontinuity of σ_{11} and σ_{22} are close to stiffer ones.

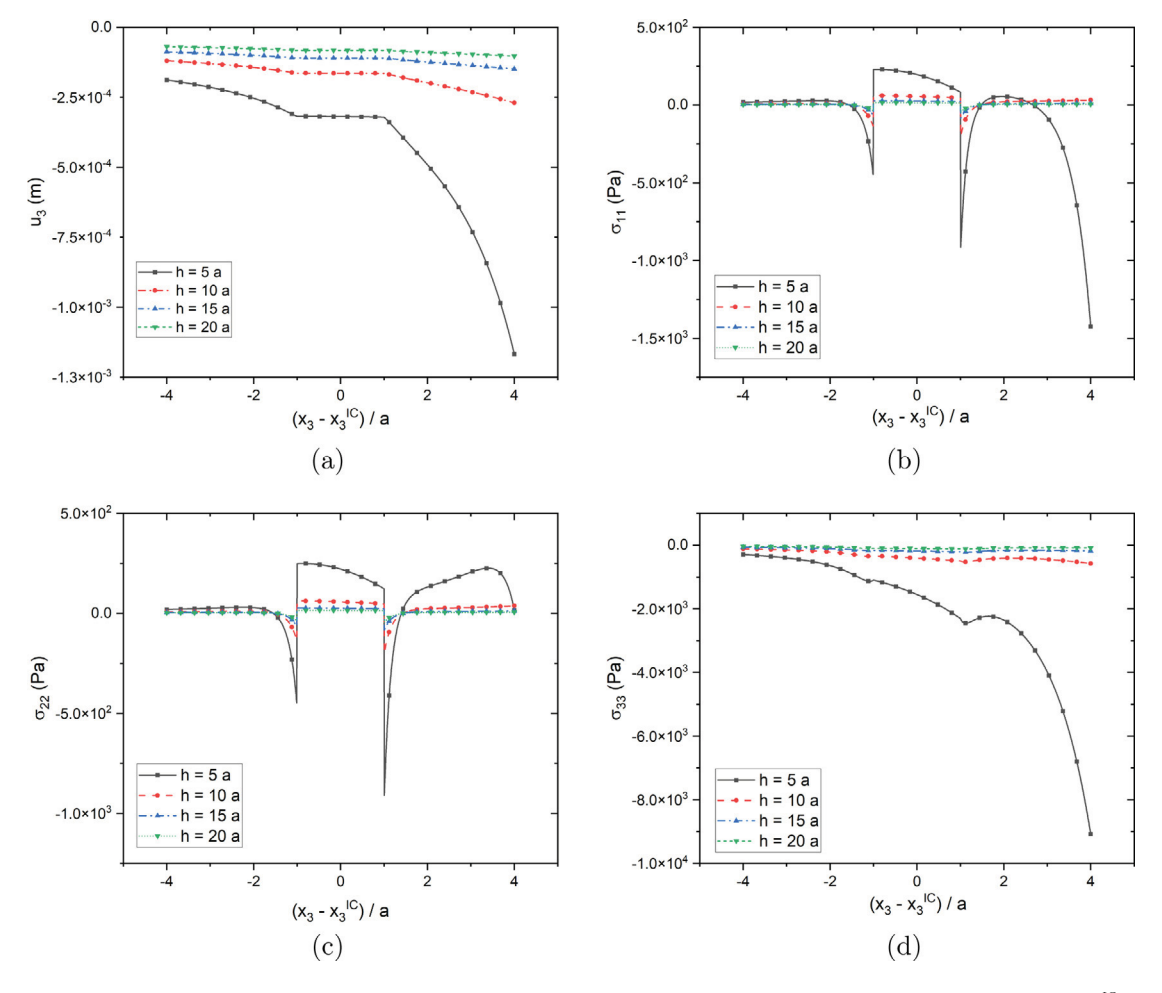


Fig. 11. The effect of the depth of the tank on: (a) u_3 and normal stresses (b) σ_{11} , (c) σ_{22} , (d) σ_{33} versus depth h along the vertical symmetric axis $x_3 - x_3^{IC} \in [-4a, 4a]$ of heat exchanger with radius a = 1.5 m under a uniform surface load $\frac{160}{9}$ kPa.

5.2. Thermal stress in the tank caused by the heat transfer

In the previous section, the effects of depth and stiffness ratios are investigated under a surface load. For heat exchangers, besides elastic disturbance, one of its purposes is to transfer heat from the roof system. Such process (Yin et al., 2021) has been explained and the heat exchanger can be treated as a heat source/sink. For a linear thermoelastic system, a heat source and heat sink are equivalent except for the opposite influence. Without the loss of any generality, assume the uniform volume heat rate $q_V = 35.37 \text{ W/m}^3$ and thus the exchanger can absorb 500W heat. The thermal properties are specified as, (i) K'' = 0.519 W/(m K) (Yumrutaş and Ünsal, 2012), A'' = 10 kPa (Campanella and Mitchell, 1968); (ii) $K^I = 10 \text{ W/(m K)}$, $A^I = 20 \text{ kPa}$ and $C^I = 10C''$. Let the earth exhibit a uniform far-field temperature (Wang et al., 2022), the temperature $T^0 = 20 \text{ °C}$ (reference temperature), the variation of temperature by the heat source and ETGs can be written as,

$$\overline{T}(\mathbf{x}) = \int_{\Omega^I} G(\mathbf{x}, \mathbf{x}') q_V(\mathbf{x}') + G_{m}(\mathbf{x}, \mathbf{x}') K(\mathbf{x}') T_m^*(\mathbf{x}') dV(\mathbf{x}')$$
(29)

and the upper phase is assumed to be perfectly conductive with $K'' = \infty$, so that the top surface of the soil is the same as the ambient temperature. The numerical verification of one inhomogeneity and two side-by-side inhomogeneities with prescribed volume heat sources are elaborated in the Supplemental Material. In the following, the thermal and elastic fields are illustrated along both the horizontal and vertical symmetric lines across the center of the tank within the range of [-4,4]a. Fig. 13(a) and (b) exhibit symmetric distributed temperature and heat flux q_1 along the horizontal line, respectively. Despite the existence of boundary effects, it has no impact on the horizontal properties, as indicated in the Green's function Eqs. (4) and (22). Subsequently, the comparison in Fig. 13(c) and (d) illustrated the boundary effects on mechanical properties on the vertical axis. Specifically, the curve h = 5a in Fig. 13(c) is not symmetric; however, when the depth h increases, boundary effects vanish rapidly, and therefore the central symmetry properties can be observed. Fig. 13(d) indicates that the boundary effects on a higher order are smaller as the four curves almost overlap with each other.

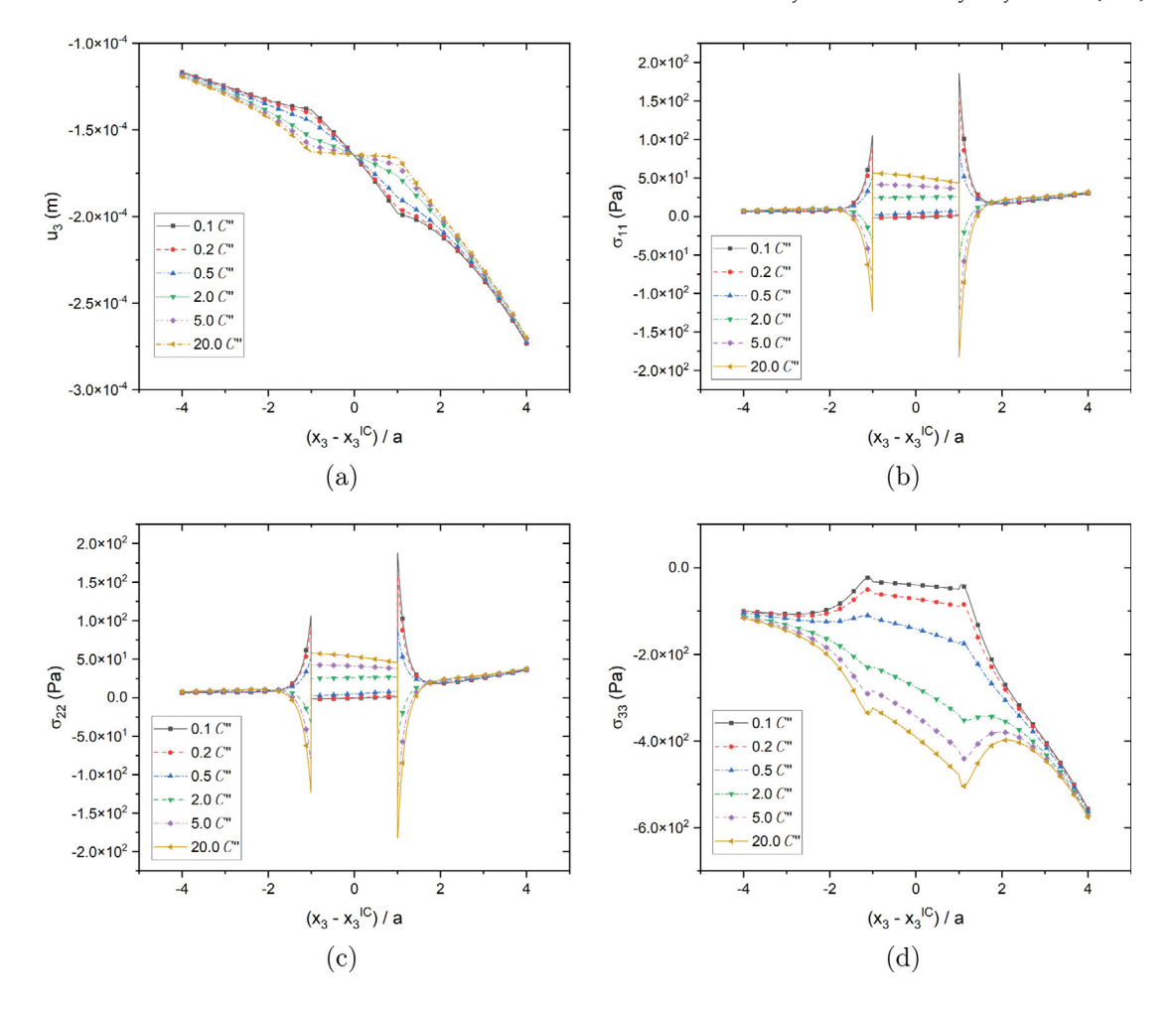


Fig. 12. The effect of the stiffness of the tank on: (a) u_3 and normal stresses (b) σ_{11} , (c) σ_{22} , (d) σ_{33} versus stiffness along the vertical symmetric axis $x_3 - x_3^{IC} \in [-4a, 4a]$ of heat exchanger with radius a = 1.5 m under a uniform surface load $\frac{160}{6}$ kPa.

Similarly, in Figs. 14 (a–c), the central symmetry with respect to the center $x_1 = x_1^{IC}$ also can be found for displacement u_1 and normal stresses σ_{11} and σ_{33} , so the boundary effect to the local field is relatively small. Due to the free-surface boundary conditions at the interface S, the displacement u_1 and normal stresses of the case h = 5a are smaller compared with the other three cases. As for properties along the vertical axis, shown in Fig. 15(d), the trends reverses at two ends (i) $x_3 = x_3^{IC} - 4a$ and (ii) $x_3 = x_3^{IC} + 4a$. Specifically, the displacement u_3 of case h = 5a is larger at (i) but smaller at (ii). However, the differences within the tank itself is narrow, which indicates the heat source effects dominate over the boundary effects. In Fig. 14(e) and (f), σ_{11} and σ_{33} exhibits similar variations that smaller stresses are observed when $x_3 - x_3^{IC}$, which is the top of the tank. Such phenomenon is mainly caused by u_1 and u_2 at the inhomogeneity interface as shown in Fig. 14(a).

In order to investigate the effects of stiffness ratio, the thermal expansion ratio is set as constant as $\mathcal{A}^I/(3\lambda^I+2\mu^I)$, so that when the Lame parameters change, the thermal modulus \mathcal{A}^I is adjusted accordingly. The original $\mathcal{A}^I=20$ kPa is selected as reference when $C^I=10C''$ and there exists a special case that when $C^I=5C''$, $\mathcal{A}^I=\mathcal{A}'=10$ kPa suggesting no misfit expansion strain. The depth h is again selected as 10a to be consistent with the previous section. During the linear elastic stage, the solution can be considered as a superposition of several components. The solution process can be considered as a combination of inhomogeneity embedded in the full-space and boundary effects of half-space. Figs. 15(a) and 15(d) plot the variation of displacement u_1 and u_3 along the horizontal and vertical symmetric line, respectively. The concept of symmetry and superposition explains the similar curves in the two figures due to dominating heat source effects and minor boundary effects. It is observed that, in Figs. 15(b–c) and 15(e–f), the normal stresses exhibit a higher order curve within the tank. Considering the curved temperature distribution in Fig. 13(a) and (c) and increasing thermal modulus, the increasing misfit stress $(\mathcal{A}^I-\mathcal{A}^0)\delta_{ij}\Delta T$ causes larger variation of normal stresses.

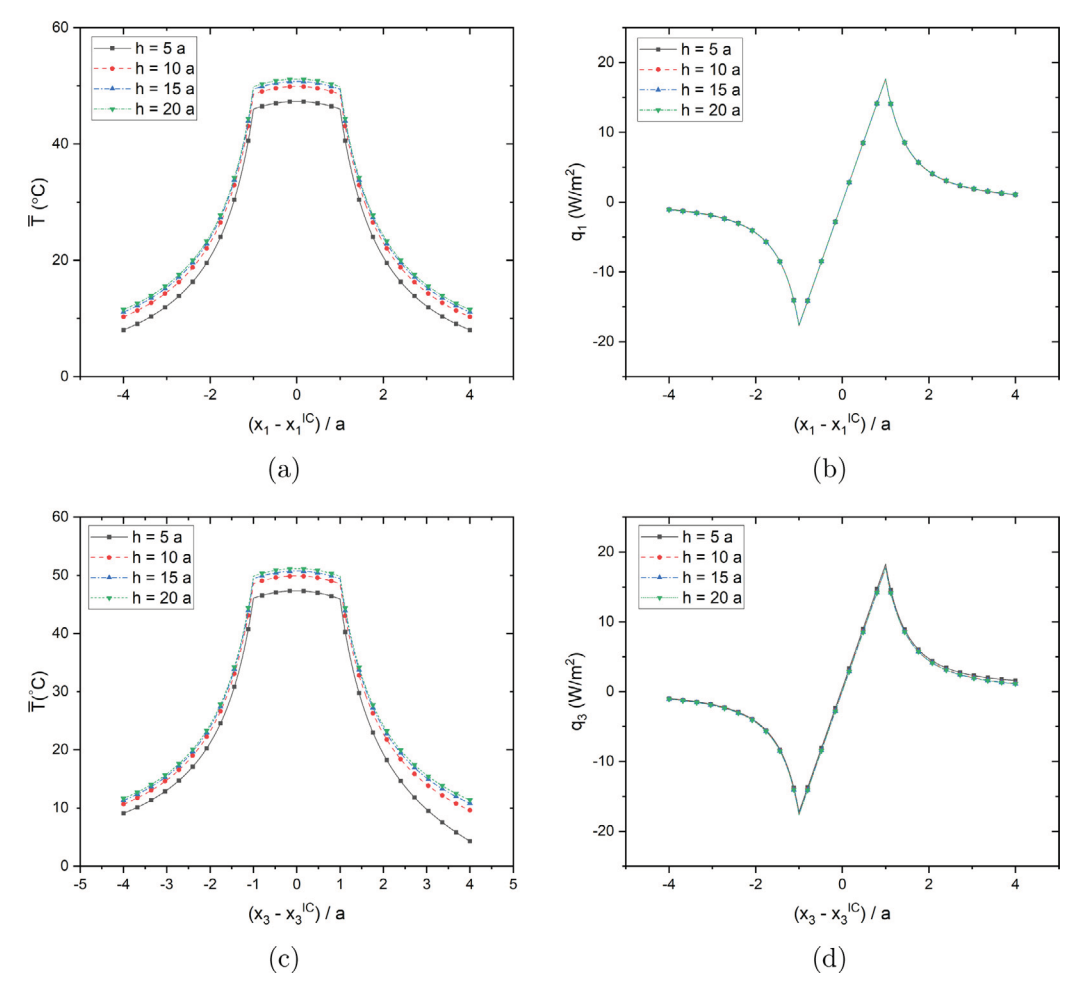


Fig. 13. The effect of the depth of the tank on: (a) \overline{T} and (b) q_1 along the horizontal symmetric axis $x_1 - x_1^{IC} \in [-4a, 4a]$; (c) \overline{T} and (d) q_3 along the vertical symmetric axis $x_3 - x_3^{IC} \in [-4a, 4a]$ of heat exchanger with radius a = 1.5 m by a volume heat source $q_v = 35.37$ W.

5.3. Effect of the tank interactions

In the geothermal industry, many geothermal heat exchangers may be installed for large-scale applications. Introducing another heat exchanger with a spacing d to an existing one can significantly change both local thermal and elastic fields due to the tank interaction, which reduces the efficiency of heat exchange and increases stress in the tank. In the field application, a large space-to-radius ratio d/a is required so that the effects brought by the heat source and material misfit on the efficiency and performance can be under control. The detailed investigation of two side-by-side and subsequently multiple heat exchangers is illustrated in Section 2 of the Supplemental Material, and a brief conclusive summary of the study is provided here. In Fig. 16, the radius a, depth h, spacing d, and volume heat source q_v of the equal-sized tanks are 1.5 m, 15 m, 9 m and 35.37 W, respectively.

In the investigation of boundary effects, Liu et al. (2015) concluded the influences of inhomogeneity with eigenstrain field vanish quickly as only 8 simple cubic distributed inhomogeneity produces a convergent solution of elastic fields. Based on the elastic bimaterial Green's function in Eq. (4) and the Eshelby's tensors, the displacement and stresses vanishes at the rate of r^{-2} and r^{-3} , respectively. Extending a similar analysis to the thermoelastic fields, the displacement and stress vanishes slower as, (i) r^0 and r^{-1} for heat sources; (ii) r^{-1} and r^{-2} for ETGs, respectively. Hence, when the number of heat exchangers increases, their disturbance to stress field of the vertical symmetry line gradually reduces, however, the displacement keeps increasing because of dimensionless Green's function.

To investigate the convergent temperature, flux, and stress fields, six cases of n = 1, 3, 9, 25, 81 and 401 heat exchangers in a row are studied and the local field of the central one is illustrated. Fig. 17(a) shows when $n \ge 25$, the temperature converges as very minor discrepancies can be observed between n = 25, 81 and n = 401. As a partial derivative of temperature, the heat flux (similar to temperature gradient) converges even faster as all curves in Fig. 17(b) exhibit small differences. Regarding to stresses, the trends of σ_{33} in Fig. 17(d) are similar to temperature in Fig. 17(a), though σ_{33} involves effects of eigenstrain, heat source and ETGs. Since the temperature differences among n = 25, 81 and n = 401 are small, the non-mechanical strain due to the temperature change converges.

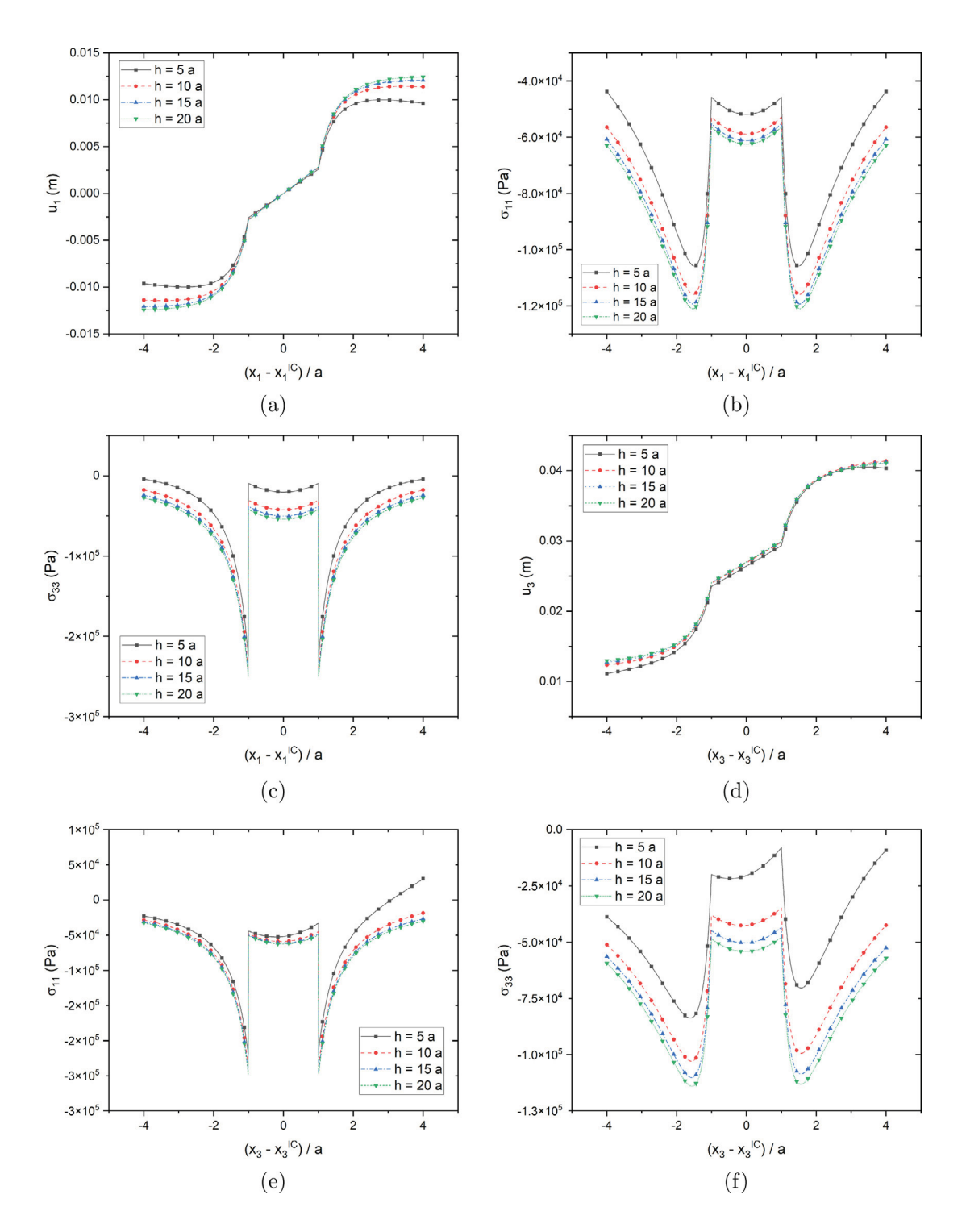


Fig. 14. The effect of the depth of the tank on: (a) u_1 , (b) σ_{11} and (c) σ_{33} along the horizontal symmetric axis $x_1 - x_1^{IC} \in [-4a, 4a]$; and (d) u_3 , (e) σ_{11} and (f) σ_{33} along the vertical symmetric axis $x_3 - x_3^{IC} \in [-4a, 4a]$ of heat exchanger with radius a = 1.5 m by a volume heat source $q_v = 35.37$ W.

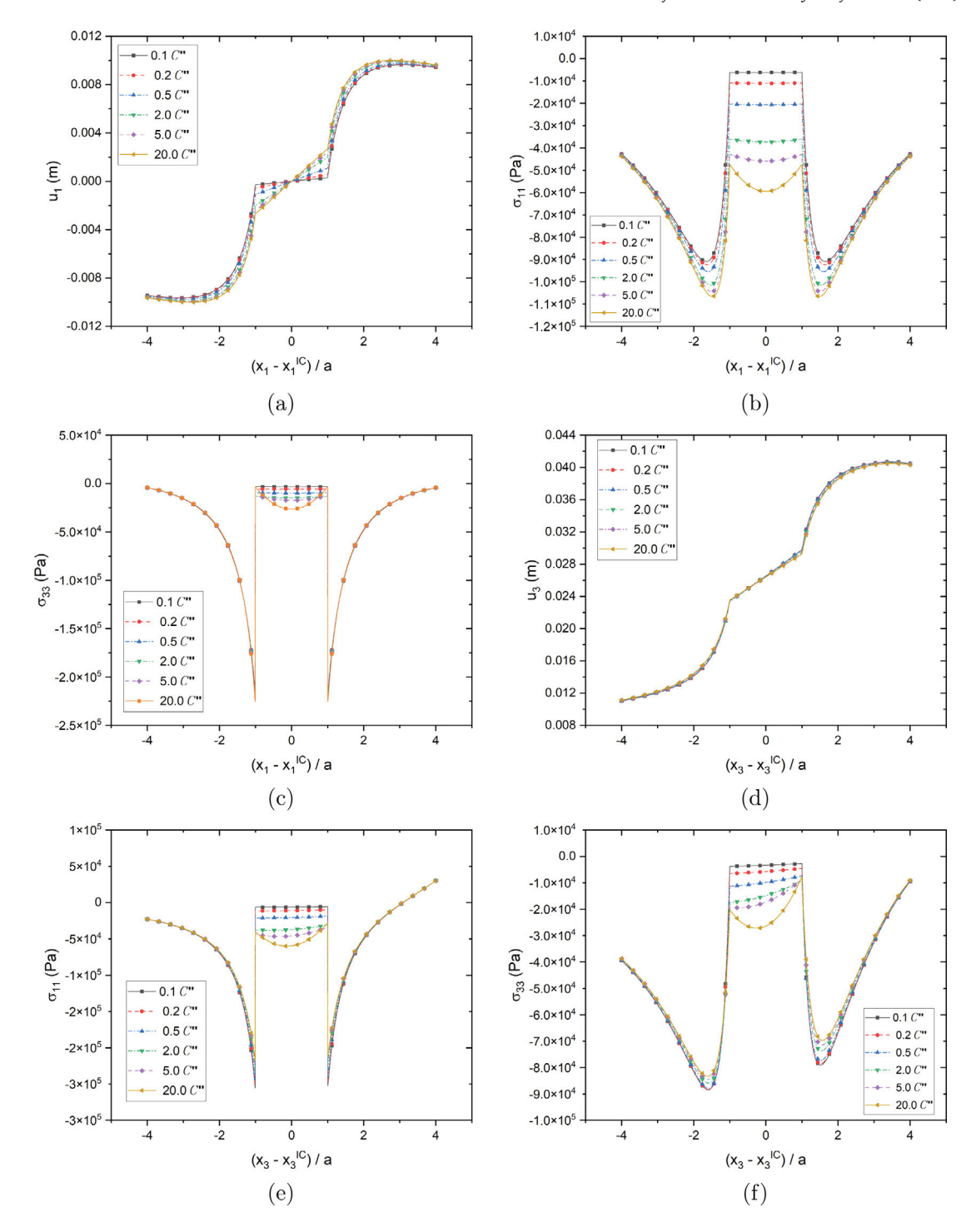


Fig. 15. The effect of the stiffness of the tank on: (a) u_1 , (b) σ_{11} and (c) σ_{33} along the horizontal symmetric axis $x_1 - x_1^{IC} \in [-4a, 4a]$; and (d) u_3 , (e) σ_{11} and (f) σ_{33} along the vertical symmetric axis $x_3 - x_3^{IC} \in [-4a, 4a]$ of heat exchanger with radius a = 1.5 m by a volume heat source $q_v = 35.37$ W.

However, the larger variance in Fig. 17(c) reveals the non-negligible role by eigenstrains. As the heat exchangers are placed along the horizontal symmetric line (x_1) , the thermal effects accumulate with more tanks, which results in a higher eigenstrain and a lower convergent rate.

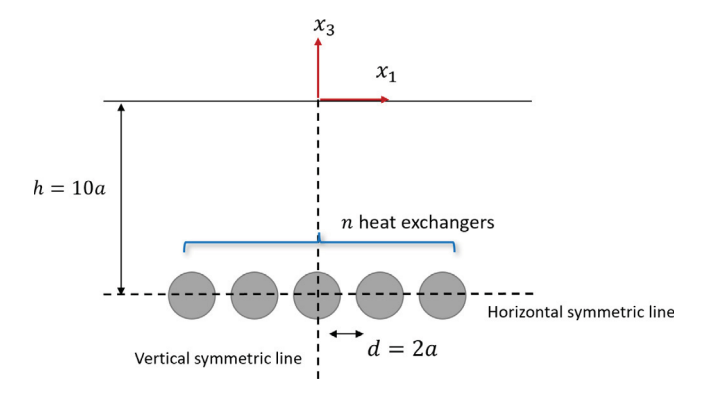


Fig. 16. Schematic illustration on a row of multiple (n) underground heat exchangers (radius a) located at depth h = 10a with distance d = 2a with volume heat source $q_v = 35.37$ W/m³.

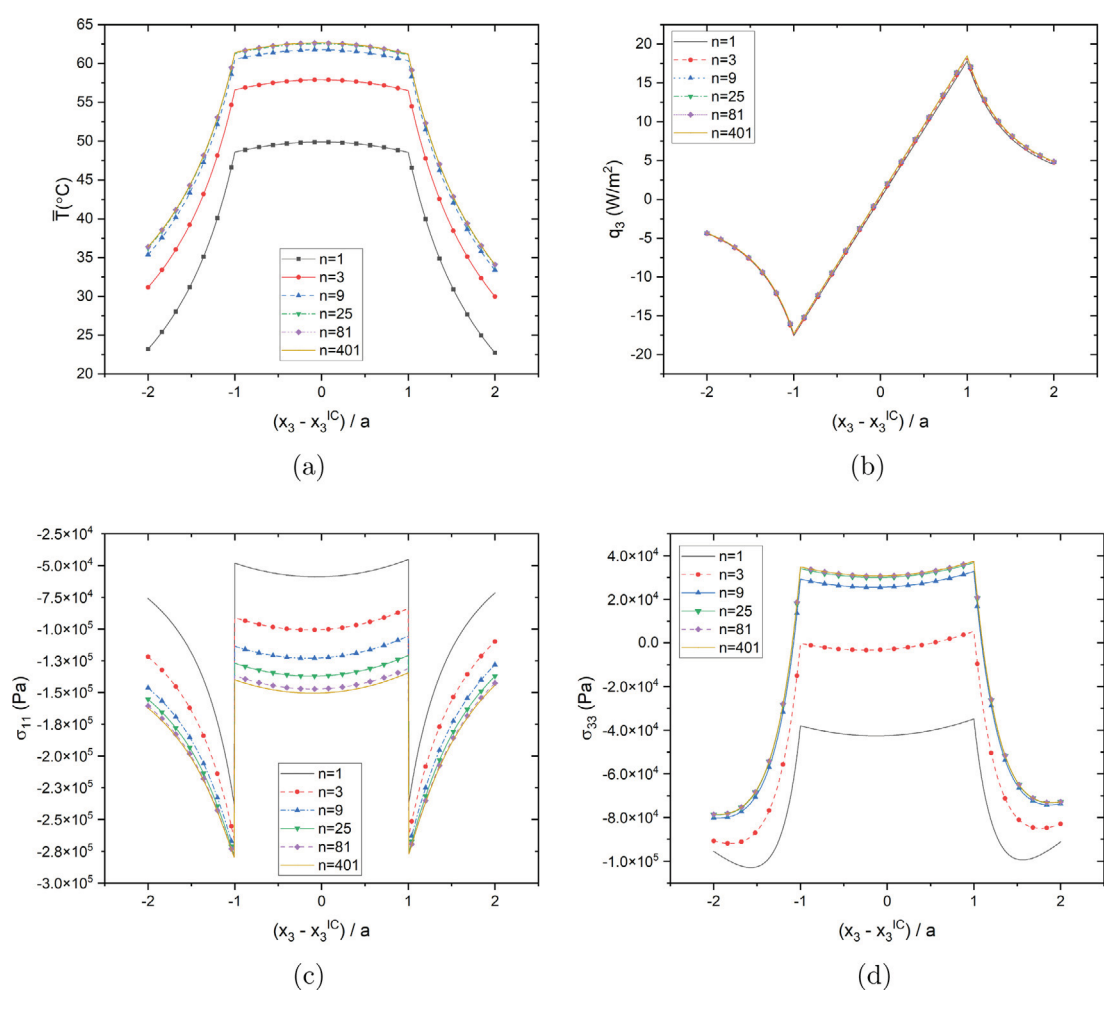


Fig. 17. The effect of the number of the tanks on: (a) \overline{T} , (b) q_3 , (c) σ_{11} and (d) σ_{33} along the vertical symmetric axis $x_3 - x_3^{IC} \in [-2a, 2a]$ under multiple n heat exchangers with radius a = 1.5 m by a volume heat source $q_v = 35.37$ W.

6. Exact solution for a single spherical heat exchanger in an infinite solid

Eshelby's EIM (Eshelby, 1957, 1959) handled with the elastic problem for an inhomogeneity in an infinite domain subjected to a uniform far field stress, which can be straightforwardly extended to multi-physical problems, such as thermal, magnetic, or

electric problems (Yin et al., 2022; Wu et al., 2021a). However, the thermoelastic problem with an inhomogeneity in an infinite domain has not been solved in the literature yet. When a heat tank is far from the surface or other tanks, the thermoelastic field in the neighborhood of the tank can be simplified by an inhomogeneity in an infinite domain. By reducing the Green's functions from bi-materials to a single homogeneous material with material constants K, C, A, certain eigen-field terms may exactly satisfy Eqs. (26) and (27) without higher order terms, which has been observed in Eshelby's EIM for an ellipsoidal inhomogeneity in an infinite domain Mura (1987), so that DEIM can provide the exact solution. Here the following two thermoelastic problems are discussed. The exactness of the solution for a spherical tank can be generalized to an ellipsoidal tank as well with the elliptical integrals (Mura, 1987).

6.1. A spherical inhomogeneity with a uniform heat source

Consider a constant heat source q^v distributed within the spherical subdomain Ω^I with K^I located at the origin point, where the far-field temperature is assumed as the reference temperature of zero. The temperature field can be easily obtained by solving Eq. (26), the ETG field is linear as shown in Eq. (30),

$$T_{ij}^{I*} = \frac{-q_v(K - K^I)}{3KK^I} \delta_{ij}$$
 (30)

which leads to the temperature field as,

$$T(\mathbf{x}) = \frac{q_v}{4\pi K} \left\{ \boldsymbol{\Phi} + \frac{K - K^I}{3K^I} \boldsymbol{\Phi}_{i,i} \right\} = \frac{q_v}{3K} \begin{cases} \frac{[a^2(4K^I - K) - |x|^2 K]}{2K^I} & |x| \le a \\ \frac{a^3}{|x|} & |x| > a \end{cases}$$
(31)

By solving Eq. (27), the thermal stress can also be derived. Because a linear ETG field generally caused quadratic disturbance of the stress field, the solution of eigenstrain is a combination of uniform and quadratic terms as follows,

$$\varepsilon_{ii}^{I*} = \overline{\varepsilon^H} \delta_{ii}$$
 (32)

and

$$\varepsilon_{ijmn}^{I*} = \overline{\varepsilon^A} \delta_{ij} \delta_{mn} + \overline{\varepsilon^B} (\delta_{im} \delta_{jn} + \delta_{jm} \delta_{in}) \tag{33}$$

where the eigenstrain parameters are written as,

$$(1+v)\alpha\Big[3(\lambda^{I}-\lambda)+2(\mu^{I}-\mu)\Big]\Big[10K^{I}\lambda^{I}\mu(1+v)+20K^{I}\mu^{I}[\lambda(1-2v)+\mu(1-v)]+K\mu\mathcal{E}+4K\lambda\mu^{I}(1-2v)+\\ 2K\mu[\lambda^{I}(1+v)+2\mu^{I}(1-v)]\Big]\\ +(\mathcal{A}-\mathcal{A}^{I})\Big[30K^{I}(1-v)\mathcal{D}+K\Big(\mu(1+v)\mathcal{E}+4\mu^{I}\mu^{I}(1-v-2v^{2})+6\mu^{I}\lambda^{I}(1-v-2v^{2})+12\mu^{I}\lambda(1-2v)(2-3v)+\\ \overline{\epsilon^{H}}=\frac{-a^{2}q_{v}\delta_{ij}}{30KK^{I}}\frac{2\mu^{I}\mu(10-28v+22v^{2})+6\mu\lambda^{I}(1-v^{2})\Big)\Big]}{\mathcal{D}\mathcal{E}}$$
 (34)

$$\overline{\varepsilon^A} = \frac{q_v(1+v)\mu(5\alpha\lambda^I - \mathcal{A}^I) + 2q_v\mu^I[(2-3v)(\mathcal{A} - \mathcal{A}^I) + (1+v)\alpha(\mu - \lambda)]}{30K^ID}$$
 (35)

and

$$\overline{\epsilon^B} = \frac{q_v(1+v)(\mu^I - \mu)\mathcal{A}^I}{30K^I \mathcal{D}}$$
(36)

in which $\mathcal{D} = (1+\nu)\mu\lambda^I + 2[(1-2\nu)\lambda + \mu(1-\nu)]\mu^I$ and $\mathcal{E} = 2(1-2\nu)(3\lambda + 2\mu) + (1+\nu)(3\lambda^I + 2\mu^I)$. Using the Eshelby's tensors **D**, **R** and **S**, the displacement can be determined as follows,

$$u_{i}(\mathbf{x}) = \frac{1}{8\pi(1-\nu)} \left\{ \frac{\alpha(1+\nu)q_{v}}{K} \left[\Psi_{,i} + \frac{K-K^{I}}{3K^{I}} \Psi_{m,im} \right] + \overline{\epsilon^{H}} \left[\Psi_{,imm} - 2(4-\nu)\boldsymbol{\Phi}_{,i} \right] \right. \\ + \overline{\epsilon^{A}} \left[\Psi_{mm,ihh} - 2(4-\nu)\boldsymbol{\Phi}_{mm,i} \right] + 2\overline{\epsilon^{B}} \left[\Psi_{mh,imh} - 2\nu\boldsymbol{\Phi}_{mm,i} - 8(1-\nu)\boldsymbol{\Phi}_{im,m} \right] \right\}$$

$$= \frac{x_{i}}{(1-\nu)} \left\{ \frac{\alpha(1+\nu)q_{v}}{90KK^{I}} \left[5a^{2}(K+2K^{I}) - 3K|x|^{2} \right] + \frac{(3-\nu)}{3}\overline{\epsilon}^{H} \\ + \frac{(3-\nu)}{5}|x|^{2}\overline{\epsilon}^{A} + \frac{2}{15} \left[5(-3+4\nu)a^{2} - 3(-6+7\nu)|x|^{2} \right] \overline{\epsilon}^{B}}{2(2K-5K^{I}) + 15a^{3}K^{I}|x|^{2}} + \frac{(3-\nu)a^{3}}{3|x|^{3}}\overline{\epsilon}^{H} \\ + \frac{(3-\nu)a^{5}}{5|x|^{3}}\overline{\epsilon}^{A} + \frac{2a^{5}(3-\nu)}{15|x|^{3}}\overline{\epsilon}^{B} \right.$$

$$\left. |x| > a \right\}$$

6.2. A spherical inhomogeneity in a uniform far field heat flux

Consider a uniform heat flux passes through a large material domain with K, C, A containing a spherical inhomogeneity Ω^I with K^I , C^I , A^I . The linear temperature distribution will be disturbed in the neighborhood of the inhomogeneity. The uniform far-field temperature gradient is given in the third direction as $\mathbf{T}^0 = [0,0,T_3^0]$, and the reference temperature is taken zero at $x_3=0$ or $T_{x_3=0}=0$, which makes the temperature distribution as an odd function of x_3 . Without the loss of any generality, let the center \mathbf{x}^{IC} locate at the origin and the reference displacement keeps zero at the origin without rigid body rotation. From the equivalent heat flux condition of Eq. (26), the uniform ETG can be determined as,

$$T_i^* = 3\delta_{i3}T_3^0 \frac{K - K^I}{2K + K^I} \tag{38}$$

and the temperature field can be obtained through the superposition of a linear one by the gradient and a disturbed one by the uniform ETG.

$$T(\mathbf{x}) = T_3^0 x_3 - \frac{\Phi_{,3} T_3^*}{4\pi} = \frac{T_3^0 x_3}{2K + K^I} \times \begin{cases} 3K & |x| \le a \\ (2K + K^I) - (K - K^I) \frac{a^3}{|x|^3} & |x| > a \end{cases}$$
 (39)

When there is no inhomogeneity, the linear temperature distribution will lead to a linear strain field as,

$$\varepsilon_{i}^{T} = \alpha T_{3}^{0} x_{3} \delta_{ij} \tag{40}$$

which is compatible without any thermal stress induced in an unconstrained domain. The corresponding displacement can be obtained through integration as follows,

$$u_i^{\infty} = \frac{\alpha T_3^0}{2} \{ 2x_i x_3 - \delta_{i3} (x_1^2 + x_2^2 + x_3^2) \}$$
 (41)

where the reference displacement is zero at the origin. The solution to the inhomogeneity problem can be decomposed into two steps, (i) determination of eigenstrain without disturbance of ETG; (ii) determination of eigenstrain caused by ETG only.

Step (i) is corresponding to the case the inhomogeneity exhibits the same thermal conductivity as the matrix, so the linear temperature distribution is not disturbed but thermal stress is still induced due to the different thermal expansion coefficient and stiffness of the tank.

Using Eq. (40) as a far field strain, $\varepsilon_{kl}^{\infty}$, in Eq. (27), we can solve the linear eigenstrain field as,

$$\varepsilon_{ijm}^{*I} = \overline{\varepsilon}^C \delta_{ij} \delta_{m3} \tag{42}$$

where

$$\overline{\varepsilon}^C = \frac{T_3^0 (1 - \nu) \left[\mathcal{A}^I - \alpha (3\lambda^I + 2\mu^I) \right]}{(1 + \nu)(3\lambda^I + 2\mu^I) - 2\nu(3\lambda + 2\mu)} \tag{43}$$

and the displacement is obtained as,

$$u_{i}(\mathbf{x}) = \frac{\alpha T_{3}^{0}}{2} \left\{ 2x_{i}x_{3} - \delta_{i3}|x|^{2} \right\} + \frac{\overline{\epsilon}^{C}}{5} \begin{cases} x_{i}x_{3} + \delta_{i3} \frac{-35a^{2} + 33|x|^{2}}{6} & |x| \leq a \\ \frac{a^{5}}{|x|^{5}} \left[x_{i}x_{3} - \frac{\delta_{i3}}{3} \right] & |x| > a \end{cases}$$

$$(44)$$

In Step (ii), the interior ($|x| \le a$) disturbed displacement by ETG in Eq. (38) can be derived as,

$$u_i^E(\mathbf{x}) = -\frac{\alpha(1+\nu)}{8\pi(1-\nu)} T_j^* \Psi_{,ij} = \frac{\alpha T_3^0 (1+\nu)(K-K^I)}{5(1-\nu)(2K+K^I)} \left[x_i x_3 + \delta_{i3} \frac{|x|^2 - 5a^2}{2} \right] \quad |x| \le a$$
(45)

It is lengthy to write the explicit form of linear eigenstrain ε_{ijm}^{*II} caused by ETG through solving the linear equation system of Eq. (27). However, it is straightforward to implement it numerically, and then solve for displacement with Green's functions. The entire solution is the superposition of far-field displacement and two linear eigenstrain, which is an exact solution without higher-order eigenstrains. The subsequent process is elaborated in Section 3 of the Supplemental Material with the "Mathematica" script.

7. Conclusions

This paper investigates the thermal, elastic, and thermoelastic problems for a spherical thermal tank in geothermal applications. The thermoelastic Green's function for a bi-material infinite domain has been re-derived in the form of a Cartesian vector, which is convenient for analytical volume integral. Using the three types of Green's function for bi-materials, the temperature and displacement fields caused by a heat source, body force, ETG, and eigenstrain, which can be in a polynomial function over a spherical subdomain, can be solved analytically. The DEIM can solve the thermal and elastic problem for a spherical thermal tank in a bi-material in a coupled way, The following significant contributions of this work are summarized:

1. The Green's functions for bi-materials are versatile and can recover the case for semi-infinite domain and infinite domain with a single material;

- 2. The DEIM provides a rapid way to solve the thermoelastic fields of a spherical heat tank in a bi-material or single-material domain, which has been verified with FEM with an excellent agreement;
- 3. The DEIM provides the exact solutions for a tank in an infinite single material with a uniform heat source or under a uniform far-field heat flux;
- 4. The DEIM is demonstrated for the geothermal system design with energy flow and stress analysis, and multi-tank interactions are illustrated.

Using Hadamard's Regularization in the x_3 direction, the present DEIM can be extended to the two-dimensional bi-material thermoelastic analysis. The accuracy of the method can be tailored by using different orders of the eigen-fields, including ETC and eigenstrain, through their Taylor series expansion at the center of each subdomain. The formulation can be extended to the ellipsoidal and arbitrary shapes of geothermal tanks. The extension of this work to finite domains with boundary effects is underway.

CRediT authorship contribution statement

Chunlin Wu: Conceptualization, Methodology, Data curation, Software, Validation, Writing – original draft, Visualization. **Tengxiang Wang:** Investigation, Writing – review & editing. **Huiming Yin:** Conceptualization, Resource, Writing – review & editing, Supervision, Funding acquisition.

Declaration of competing interest

The authors declare that they have no known competing financial interests or personal relationships that could have appeared to influence the work reported in this paper.

Data availability

Data will be made available on request.

Acknowledgments

This work is sponsored by the National Science Foundation, United States IIP #1738802, IIP #1941244, CMMI#1762891, and U.S. Department of Agriculture, United States NIFA #2021-67021-34201 whose support is gratefully acknowledged. We also thank Dr. Liangliang Zhang from China Agricultural University on the discussion of verification, whose help is gratefully acknowledged.

Appendix A. Determination of coefficients $\overline{A}_{11} \cdots A'_{22}$

This appendix provides details to construct equations for Eq. (15) in Section 3.2.

(1) Using the continuity condition of u_1 and u_2 , the upper phase,

$$2\mu' u_i = (A_{11} + \overline{A}_{11})\beta^u_i + (A_{12} - \overline{A}_{12})\alpha^u_i$$

and in the lower phase,

$$2\mu''u_i = A'_{11}\beta^u_i + A'_{12}\alpha^u_i$$

(2) Using the continuity condition of u_3 , the upper phase,

$$2\mu'u_3 = (A_{11} - \overline{A}_{11})\beta_3^u + (A_{12} + \overline{A}_{12})\alpha_3^u - (3 - 4\nu')\{(A_{21} - \overline{A}_{21})\alpha^u + \overline{A}_{22}\phi\} + 4(1 - \nu')\{(A_3 - \overline{A}_3)\alpha^u\}$$

and in the lower phase,

$$2\mu''u_3 = A_{11}'\rho_{,3}^u + A_{12}'\alpha_{,3}^u - (3 - 4\nu'')\{A_{21}'\alpha^u + A_{22}'\phi\} + 4(1 - \nu'')A_3'\alpha^u$$

(3) Using the continuity condition of γ_{31} and γ_{32} , the upper phase,

$$\tau_{13} = (A_{11} - \overline{A}_{11})\beta_{13}^{u} + (A_{12} + \overline{A}_{12})\alpha_{13}^{u} - (1 - 2\nu')\{(A_{21} - \overline{A}_{21})\alpha_{1}^{u} + \overline{A}_{22}\phi_{.1}\} + 2(1 - \nu')\{(A_{3} - \overline{A}_{3})\alpha_{1}^{u}\}$$

and in the lower phase,

$$\tau_{13} = A'_{11}\beta''_{,13} + A'_{12}\alpha''_{,13} - (1 - 2\nu'')\{A'_{21}\alpha''_{,1} + A'_{22}\phi_{,1}\} + 2(1 - \nu'')\{A'_{3}\alpha''_{,1}\}$$

(4) Using the continuity condition of σ_{33} , the upper phase,

$$\sigma_{33} = (A_{11} + \overline{A}_{11})\beta_{33}^{u} + (A_{12} - \overline{A}_{12})\alpha_{33}^{u} - 2(1 - v')\{(A_{21} + \overline{A}_{21})\alpha_{3}^{u} - \overline{A}_{22}\phi_{,3}\} + 2(1 - v')(A_{3} + \overline{A}_{3})\alpha_{3}^{u}$$

and in the lower phase,

$$\sigma_{33} = A'_{11}\beta^{u}_{,33} + A'_{12}\alpha^{u}_{,33} - 2(1 - \nu'')\{A'_{21}\alpha^{u}_{,3} + A'_{22}\phi_{,3}\} + 2(1 - \nu'')A'_{3}\alpha^{u}_{,3}$$

Collecting the equivalent terms in the 4 equivalent conditions, eight equations can be constructed as Eq. (15).

Appendix B. Green's functions for semi-infinite domains and an infinite homogeneous domain

B.1. Semi-infinite domain with a Neumann's boundary condition on the surface

When one material phase is reduced to a vacuum with K' = C' = 0, the infinite bi-material is reduced to a semi-infinite single material domain with a Neumann's boundary condition of a free surface from heat flux and traction. The Green's functions are obtained as follows for both source and field points in \mathcal{D}^- .

(i) Thermal Green's function

$$G(\mathbf{x}, \mathbf{x}') = \frac{1}{4\pi K''} (\phi + \overline{\phi})$$
(B.1)

(ii) Elastic Green's function

$$4\pi\mu''G_{ij}(\mathbf{x},\mathbf{x}') = (\delta_{ij}\phi - \frac{\psi_{,ij}}{4(1-\nu'')}) + \overline{\phi}\delta_{ij} - 2(\delta_{i3}\delta_{jk} - \delta_{ik}\delta_{j3})\overline{\alpha}_{,k}^{l}$$

$$- \frac{1}{2(1-\nu'')}x_{3} \left[Q_{J}\overline{\psi}_{,ij3} + 4(1-\nu'')\delta_{j3}\overline{\phi}_{,i} + 2(1-2\nu'')\delta_{i3}Q_{J}\overline{\phi}_{,j} - Q_{J}x_{3}\overline{\phi}_{,ij}\right]$$

$$- \frac{3-4\nu''}{4(1-\nu'')}Q_{I}Q_{J}\overline{\psi}_{,ji} - (1+2\nu'')Q_{J}\overline{\beta}_{,ij}^{l}$$
(B.2)

where $A^l=1, B^l=2, C^l=\frac{1}{2(1-\nu'')}, D^l=\frac{3-4\nu''}{4(1-\nu'')}, G^l=2\nu''-1$ are applied. (iii) Thermoelastic Green's function

$$16\pi\mu'' \frac{(1-\nu'')K''}{(1-2\nu'')A''}G_{i}(\mathbf{x},\mathbf{x}') = A_{3}^{l}\psi_{,i} + 2A_{3}^{l}(1-\nu'')\overline{\beta}_{,i}^{l} + A_{3}^{l}(3-4\nu'')\overline{\psi}_{,i}$$

$$+ x_{3}A_{3}^{l} \left[4(1-\nu'')\overline{a}_{,i}^{l} + 2(\overline{\psi}_{,i3} + 2(1-2\nu'')\delta_{i3}\overline{\phi} - x_{3}\overline{\phi}_{,i}) \right]$$

$$+ \delta_{i3}A_{3}^{l} \left[-(3-4\nu'')(-\overline{a}^{l} + 2\overline{\psi}_{,3}) - \overline{a}^{l} \right]$$
(B.3)

where $A_3^l = \overline{A_3}^l$, $A_3^{l'} = 0$, $L_B^l = A_3^l (3 - 4v'')$, $L_C^l = 2A_3^l$, $L_D^l = 0$, $L_F^l = 4(1 - v'')A_3^l$ and $\overline{A_{11}}^l = (2v'' - 1)A_3^l$, $\overline{A_{21}}^l = -A_3^l$ are applied.

B.2. Semi-infinite domain with a Dirichlet's boundary condition on the surface

When one material phase is reduced to an ideally rigid thermal conductor with $K' \to \infty$, A = 0, and $C' \to \infty$, the infinite bi-material is reduced to a semi-infinite single material domain exhibiting a Dirichlet's boundary condition with a fixed uniform temperature and displacement along the surface. The Green's functions are obtained as follows for both source and field points in

(i) Thermal Green's function

$$G(\mathbf{x}, \mathbf{x}') = \frac{1}{4\pi K''} (\phi - \overline{\phi})$$
(B.4)

(ii) Elastic Green's function

$$4\pi\mu''G_{ij}(\mathbf{x},\mathbf{x}') = (\delta_{ij}\phi - \frac{\psi_{,ij}}{4(1-\nu'')}) - \overline{\phi}\delta_{ij} + \frac{1}{4(1-\nu'')}Q_{I}Q_{J}\overline{\psi}_{,ji} + \frac{x_{3}}{2(1-\nu'')(3-4\nu'')} \left[Q_{J}\overline{\psi}_{,ij3} + 4(1-\nu'')\delta_{j3}\overline{\phi}_{,i} + 2(1-2\nu'')\delta_{i3}Q_{J}\overline{\phi}_{,j} - Q_{J}x_{3}\overline{\phi}_{,ij}\right]$$
(B.5)

where $A^l=-1, B^l=0, C^l=\frac{-1}{2(1-\nu'')(3-4\nu'')}, D^l=\frac{-1}{4(1-\nu'')}, G^l=0$ are applied. (iii) Thermoelastic Green's function

$$16\pi\mu'' \frac{(1-\nu'')K''}{(1-2\nu'')A''}G_{i}(\mathbf{x},\mathbf{x}') = \psi_{,i} - \frac{2x_{3}}{3-4\nu''} \left[\left(\overline{\psi}_{,i3} + 2(1-2\nu'')\delta_{i3}\overline{\phi} - x_{3}\overline{\phi}_{,i} \right) \right] + \delta_{i3} \left[(3-4\nu^{q})\overline{\alpha}^{y} + 2\overline{\psi}_{,3} + (3-4\nu'')\overline{\alpha}^{y} \right]$$
(B.6)

where $A_3^l = -\overline{A_3}^l, A_3^{l'} = 0, \ L_B^l = -A_3^l, L_C^l = \frac{-2}{3-4\nu''}A_3^l, L_D^l = -\frac{4(1-\nu'')}{3-4\nu''}A_3^l, L_F^l = -\frac{4(1-\nu'')}{3-4\nu''}A_3^l$ and $\overline{A}_{11}^l = A_3^l, \overline{A}_{21}^l = -A_3^l$ are applied.

B.3. Green's functions for an infinite domain with a homogeneous material

When two material phases are identical, the Green's functions are simplified as follows,

(i) Thermal Green's function

$$G(\mathbf{x}, \mathbf{x}') = \frac{\phi}{4\pi K} \tag{B.7}$$

(ii) Elastic Green's function

$$G_{ij}(\mathbf{x}, \mathbf{x}') = \frac{\delta_{ij}\phi}{4\pi\mu(1-\nu)} - \frac{\psi_{,ij}}{16\pi\mu(1-\nu)}$$
(B.8)

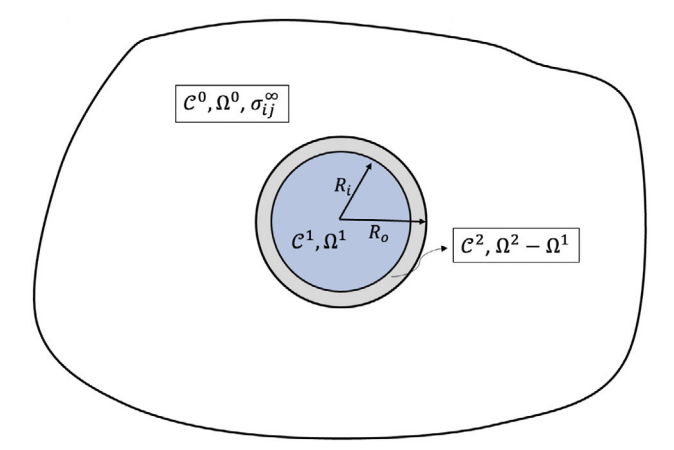


Fig. C.18. A hollow ball filled with a liquid inside an infinite domain under a far-field uniform test load.

(iii) Thermoelastic Green's function

$$G_i(\mathbf{x}, \mathbf{x}') = \frac{\alpha(1+\nu)}{8\pi K(1-\nu)} \psi_{,i}$$
(B.9)

Appendix C. Estimation of the effective mechanical properties of a spherical thermal tank

This subsection aims to provide details on the estimation of effective mechanical properties of the spherical geothermal tank. During working conditions, the spherical thermal tank is filled with water, which can be homogenized as a uniform solid ball with a certain effective stiffness. Specifically, in most cases, the tank may not be full. In such a case, a partially full tank may exhibit the same effective stiffness as an empty tank when the inner pressure is negligible. The effective stiffness of a spherical thermal tank can be estimated through the double-inclusion model proposed by Hori and Nemat-Nasser (1993). Assume the thickness of the thermal water tank is uniform, shown in Fig. C.18, the ball Ω^2 is composed of (i) space for liquid Ω^1 and (ii) a uniform thin spherical shell $\Omega^2 - \Omega^1$. Let R_o and R_i denote the outer and inner radius, and Ω^1 and $\Omega^2 - \Omega^1$ are filled with isotropic material with stiffness C^1 and C^2 , respectively.

Now embed this ball in an infinite domain Ω^0 with stiffness C^0 , and apply a uniform test load σ_{ij}^{∞} (or equivalently $\varepsilon_{ij}^{\infty}$) in the far field. Since the geometry of the thermal tank and the space for liquid are coaxial and similar, ΔS terms vanish in Eq.(3.6 a, b) of Hori and Nemat-Nasser (1993). Therefore, the effective stiffness tensor can be written as,

$$\overline{C}^{lank} = C^{0} : \{ \mathbf{I} + (S^{2} - \mathbf{I}) : \boldsymbol{\Phi}^{R} \} : \{ \mathbf{I} + S^{2} : \boldsymbol{\Phi}^{R} \}
\boldsymbol{\Phi}^{1} = -\{ S^{1} + (C^{1} - C^{0})^{-1} : C^{0} \}^{-1}
\boldsymbol{\Phi}^{2} = -\{ S^{2} + (C^{2} - C^{0})^{-1} : C^{0} + \frac{f}{1 - f} \}^{-1}$$
(C.1)

where $\Phi^R = f\Phi^1 + (1-f)\Phi^2$ and $f = \frac{V^1}{V^2}$; V_1 and V_2 are the inner volume and entire volume of the thermal tank; S^1 and S^2 are uniform Eshelby's tensors associated with source domain Ω^1 and Ω^2 , respectively. Notice that the S^1 , S^2 only involve interior field points, and thus S^1 and S^2 are the exactly same constants. Obviously, the estimation of effective stiffness is dependent on the mechanical properties of the matrix C^0 and the geometry of the thermal tank.

Without the loss of any generality, let the soil be unsaturated clay and its Young's modulus and Poisson's ratio are 20 MPa and 0.3, respectively; the spherical shell of the thermal tank is made of structural steel (Young's modulus 200 GPa and Poisson's ratio 0.3); the volume fraction $f = (0.9)^3 = 0.723$. (i) When the thermal tank is empty, the effective moduli are 7.402 MPa and 0.176; (ii) when the thermal tank is filled with water (Bulk Modulus 2.1 GPa and Poisson's ratio 0.5), the effective moduli are 9.434 MPa and 0.499452.

According to Herve (2002), the effective thermal conductivity \overline{K} of a two-layered structure is,

$$\overline{K} = K^2 + \frac{K^2 f}{\frac{K^2}{K^1 - K^2} + \frac{1}{3}(1 - f)}$$
 (C.2)

and the effective thermal expansion ratio is

$$\overline{\alpha} = f\alpha^{1} + (1 - f)\alpha^{2} + (\alpha^{1} - \alpha^{2}) \frac{4\mu^{2} f(1 - f)(\Theta^{1} - \Theta^{2})^{2}}{(3\Theta^{2} + 4\mu^{2})\Theta^{1} + 4\mu^{2}(1 - f)(\Theta^{2} - \Theta^{1})}$$
(C.3)

where Θ^I is the Bulk modulus of the Ith phase; f is the volume ratio of the two subdomain defined above.

Appendix D. Supplementary data

Supplementary material related to this article can be found online at https://doi.org/10.1016/j.jmps.2023.105207.

References

Barber, J.R., 1992. Elasticity. Springer Dordrecht, Dordrecht.

Benzaama, MH, Menhoudj, S, Kontoleon, KJ, Mokhtari, AM, Lekhal, MC, 2018. Investigation of the thermal behavior of a combined geothermal system for cooling with regards to Algeria's climate. Sustainable Cities Soc. 43, 121–133.

Biot, M.A., 1956. Thermoelasticity and irreversible thermodynamics. J. Appl. Phys. 27 (3), 240-253.

Boussinesq, J., 1885. Applications Des Potentiels à L'étude de L'équilibre Et Du Mouvement Des Solides Élastiques. Gauthier-Villars.

Campanella, Richard G., Mitchell, James K., 1968. Influence of temperature variations on soil behavior. J. Rock Mech. Geotechn. Eng. 94 (3).

Chen, W.Q., Ding, H.J., Ling, D.S., 2004. Thermoelastic field of a transversely isotropic elastic medium containing a penny-shaped crack: exact fundamental solution. Int. J. Solids Struct. 41 (1), 69–83.

Collins, W.D., 1960. Some elastic and thermoelastic stress distributions in a semi-infinite solid. Mathematika 7 (2), 149-160.

Dong, Qingbing, Li, Yan, Wei, Jing, Lu, Fengxia, 2020. Layered structures with rough surfaces and interfaces at contact loading. Int. J. Mech. Sci. 178, 105611. Eshelby, John Douglas, 1957. The determination of the elastic field of an ellipsoidal inclusion, and related problems. Proc. R. Soc. Lond. Ser. A. Math. Phys. Sci. 241 (1226), 376–396.

Eshelby, John Douglas, 1959. The elastic field outside an ellipsoidal inclusion. Proc. R. Soc. Lond. Ser. A. Math. Phys. Sci. 252 (1271), 561-569.

Gao, Xiao-Wei, 2003. Boundary element analysis in thermoelasticity with and without internal cells. Internat. J. Numer. Methods Engrg. 57 (7), 975-990.

Goodier, J.N., 1937. A general proof of Saint-Venant's principle. Lond. Edinb. Dublin Philos. Mag. J. Sci. 23 (155), 607-609.

Haojiang, Ding, Fenglin, Guo, Pengfei, Hou, 2000. General solutions of coupled thermoelastic problem. Appl. Math. Mech. 21 (6), 631-636.

Hatta, H., Taya, M., 1986. Equivalent inclusion method for steady state heat conduction in composites. Internat. J. Engrg. Sci. 24, 1159-1170.

Head, A.K., 1953. Edge dislocations in inhomogeneous media. Proc. Phys. Soc. Sect. B 66 (9), 793-801.

Herve, E., 2002. Thermal and thermoelastic behaviour of multiply coated inclusion-reinforced composites. Int. J. Solids Struct. 39.

Hori, Muneo, Nemat-Nasser, Sia, 1993. Double-inclusion model and overall moduli of multi-phase composites. J. Eng. Mater. Des. 116.

Hou, Peng-Fei, Jiang, Hai-Yang, Li, Qiu-Hua, 2013a. Three-dimensional steady-state general solution for isotropic thermoelastic materials with applications I: General solutions. J. Therm. Stresses 36 (7), 727–747.

Hou, Peng-Fei, Leung, Andrew Y.T., Chen, Chang-Ping, 2008a. Fundamental solution for transversely isotropic thermoelastic materials. Int. J. Solids Struct. 45 (2), 392–408.

Hou, Peng-Fei, Leung, Andrew Y.T., He, Yong-Jun, 2008b. Three-dimensional Green's functions for transversely isotropic thermoelastic bimaterials. Int. J. Solids Struct. 45 (24), 6100–6113.

Hou, Peng-Fei, Li, Qiu-Hua, Jiang, Hai-Yang, 2013b. Three-dimensional steady-state general solution for isotropic thermoelastic materials with applications II: Green's functions for two-phase infinite body. J. Therm. Stresses 36 (8), 851–867.

Huang, Kefu, Wang, Minzhong, 1991. Elastic fundamental solutions to two jointed half-spaces. Sci. China Ser. A Math. Phys. Astron. Technol. Sci. (in Chinese) 21 (1), 41–46.

Hwang, Se-Yun, Kim, Min-Seok, Lee, Jang-Hyun, 2020. Thermal stress analysis of process piping system installed on LNG vessel subject to hull design loads. J. Mar. Sci. Eng. 8 (11).

Kramer, C.A., Basu, P., 2014. Performance of a model geothermal pile in sand. In: Gaudin, C., White, D. (Eds.), Proc. 8th Int. Conf. on Physical Modelling in Geotechnics, Perth. CRC Press/Balkema, Leiden, pp. 771–777.

Kuang, Y.H., Wang, R.Z., Yu, L.Q., 2003. Experimental study on solar assisted heat pump system for heat supply. Energy Convers. Manage. 44 (7), 1089–1098. Li, Shuhong, Dong, Kefeng, Wang, Jinyong, Zhang, Xiaosong, 2015. Long term coupled simulation for ground source heat pump and underground heat exchangers. Energy Build. 106, 13–22, SI: IEA-ECES Annex 31 Special Issue on Thermal Energy Storage.

Liu, Y.J., Mukherjee, S., Nishimura, N., Schanz, M., Ye, W., Sutradhar, A., Pan, E., Dumont, N.A., Frangi, A., Saez, A., 2011. Recent advances and emerging applications of the boundary element method. Appl. Mech. Rev. 64 (3).

Liu, Y.J., Song, G., Yin, H.M., 2015. Boundary effect on the elastic field of a semi-infinite solid containing inhomogeneities. Proc. R. Soc. A Math. Phys. Eng. Sci. 471 (2179), 20150174.

Lorentz, Hendrik Antoon, 1907. Ein allgemeiner Satz, die Bewegung einer reibenden Flüssigkeit betreffend, nebst einigen Anwendungen desselben. Abh. Theor. Phys. 1, 23.

Love, A.E.H., 2013. A Treatise on the Mathematical Theory of Elasticity. Cambridge University Press.

Michell, J.H., 1899. The transmission of strees across a plane of discontinuity in an isotropic elastic solid, and the potential solutions for a plane boundary. Proc. Lond. Math. Soc. s1-31 (1), 183–192.

Mindlin, Raymond D., 1936. Force at a point in the interior of a semi-infinite solid. Physics 7 (5), 195-202.

Mindlin, Raymond D., Cheng, David H., 1950a. Nuclei of strain in the semi-infinite solid. J. Appl. Phys. 21 (9), 926-930.

Mindlin, Raymond D., Cheng, David H., 1950b. Thermoelastic stress in the semi-infinite solid. J. Appl. Phys. 21 (9), 931-933.

Mura, Toshio, 1987. Micromechanics of Defects in Solids. Springer Netherlands, Dordrecht.

Nowacki, Witold, 1986. Thermoelasticity, second ed. Pergamon Press, OXford.

Podil'chuk, Yu. N., Sokolovskii, Ya. I., 1994. Thermostress in an infinite transversally isotropic medium with an internal elliptical crack. Int. Appl. Mech. 30 (11), 834–840.

Prasad, N.N.V., Aliabadi, M.H., Rooke, D.P., 1994. The dual boundary element method for thermoelastic crack problems. Int. J. Fract. 66 (3), 255-272.

Qu, Ming, Yin, Hongxi, Archer, David H., 2010. A solar thermal cooling and heating system for a building: Experimental and model based performance analysis and design. Sol. Energy 84 (2), 166–182.

Rongved, Leif, 1955a. Force at point in the interior of a semi-infinite solid with fixed boundary. J. Appl. Mech..

Rongved, L., 1955b. Force interior to one of two joined semi-infinite solid. In: Proc., 2nd Midwest Conf. Solid Mech.. pp. 1-13.

Sen, Bibhutibhusan, 1951. Note on the stresses produced by nuclei of thermo-elastic strain in a semi-infinite elastic solid. Quart. Appl. Math. 8 (4), 365-369.

Sharma, Brahmadev, 1958. Thermal stresses in transversely isotropic semi-infinite elastic solids. J. Appl. Mech. Trans. ASME 25 (1).

Singh, S.J., Kumari, G., Singh, K., 1999. Displacements and stresses due to a single force in a half-space in welded contact with another half-space. Geophys. J. Int. 139 (2), 591–596.

Tinti, Stefano, Armigliato, Alberto, 1998. Single-force point-source static fields: an exact solution for two elastic half-spaces. Geophys. J. Int. 135 (2), 607–626. Verruijt, A., 1969. The completeness of Biot's solution of the coupled thermoelastic problem. Quart. Appl. Math. 26 (4), 485–490.

Walpole, L.J., 1996. An elastic singularity in joined half-spaces. Internat. J. Engrg. Sci. 34 (6), 629-638.

Wang, Tengxiang, Wu, Chunlin, Zhang, Liangliang, Yin, Huiming, 2022. The green's function-based thermal analysis of a spherical geothermal tank in a semi-infinite domain. J. Appl. Mech. 89 (7), 071008.

- Wei, Rongbing, Wu, Renbing, Zhou, Kun, 2016. Fatigue crack propagation in heterogeneous materials under remote cyclic loading. J. Micromechanics Mol. Phys. 01 (01), 1650003.
- Wu, Chunlin, Wei, Zhenhua, Yin, Huiming, 2021a. Virtual and physical experiments of encapsulated phase change material embedded in building envelopes. Int. J. Heat Mass Transfer 172, 121083.
- Wu, Chunlin, Zhang, Liangliang, Cui, Junhe, Yin, Huiming, 2022. Three dimensional elastic analysis of a bi-material system with a single domain boundary element method. Eng. Anal. Bound. Elem..
- Wu, Chunlin, Zhang, Liangliang, Yin, Huiming, 2021b. Elastic solution of a polyhedral particle with a polynomial eigenstrain and particle discretization. J. Appl. Mech. 1–35.
- Wu, Chunlin, Zhang, Liangliang, Yin, Huiming, 2023. Stress concentration of a micro-void embedded in a bi-layered material considering the boundary effects. J. Eng. Mech. 149.
- Yin, Huiming, Song, Gan, Zhang, Liangliang, Wu, Chunlin, 2022. The Inclusion-Based Boundary Element Method (IBEM). Academic Press.
- Yin, H.M., Yang, D.J., Kelly, G., Garant, J., 2013. Design and performance of a novel building integrated PV/thermal system for energy efficiency of buildings. Sol. Energy 87, 184–195.
- Yin, Huiming, Zadshir, Mehdi, Pao, Frank, 2021. Building Integrated Photovoltaic Thermal Systems: Fundamentals, Designs and Applications. Academic Press.
- Yu, H.Y., Sanday, S.C., 1991. Elastic fields in joined half-spaces due to nuclei of strain. Proc. R. Soc. Lond. Ser. A Math. Phys. Sci. 434 (1892), 503–519.
- Yu, H.Y., Sanday, S.C., Rath, B.B., 1992. Thermoelastic stresses in bimaterials. Phil. Mag. A 65 (5), 1049-1064.
- Yumrutaş, Recep, Ünsal, Mazhar, 2012. Energy analysis and modeling of a solar assisted house heating system with a heat pump and an underground energy storage tank. Sol. Energy 86 (3), 983–993.
- Zhou, Kun, Hoh, Hsin Jen, Wang, Xu, Keer, Leon M., Pang, John H.L., Song, Bin, Wang, Q. Jane, 2013. A review of recent works on inclusions. Mech. Mater. 60, 144–158.
- Zhou, Kun, Keer, Leon, Wang, Q. Jane, 2011a. Analysis of hard coatings on a substrate containing inhomogeneities. J. Mech. Mater. Struct. 6 (1–4), 627–639. Zhou, Kun, Keer, Leon M., Wang, Q. Jane, 2011b. Semi-analytic solution for multiple interacting three-dimensional inhomogeneous inclusions of arbitrary shape in an infinite space. Internat. J. Numer. Methods Engrg. 87 (7), 617–638.